CODEN:LUTEDX/(TEIE-5388)/1-79(2017)

Industrial Electrical Engineering and Automation

Energy Harvesting for Electronic Systems

Oscar Ridell

Pål Nilsson

Division of Industrial Electrical Engineering and Automation
Faculty of Engineering, Lund University

Energy Harvesting for Electronic Systems

Oscar Ridell & Pål Nilsson

Lund University Faculty of Engineering

2017

Abstract

Energy harvesting enables products to become more self-sufficient of power and offers the possibility to avoid battery exchange and power cables. The performance and applicability of the most promising or popular small scale energy harvesting technologies are investigated in this thesis. The focus lies on the amount of potential energy that can be harvested and how limited the technology is to a specific environment. Different power management and energy storage methods are also examined.

Two prototypes demonstrating different energy harvesting phenomena are presented. The first prototype is able to harvest an average of 152 µW at 302-346 lux using 4 AM-1417 photovoltaic cells with an area of 19.46 cm^2. The 302-346 lux span is measured in indoor fluorescent office lighting. The second prototype uses a DC motor to harvest the energy from the motion of opening a door. It is possible to harvest more than 470 µJ from a single door opening with the prototype. This requires a minimum average revolving speed of 7.5 rpm during the door opening.

The thesis concludes that photovoltaic cells are relatively easy to use in practice and that an environment with sufficient energy is not difficult to find. Piezoelectricity and vibration based electromagnetism has a low applicability due to the fact that the transducers only gain a useful power output at their resonance frequency. However, electromagnetic pushbuttons or rotation generators are proven to be useful. Thermoelectric elements are highly dependent on specific thermal conditions, making them applicable in some cases but hard to use as an all-round energy harvesting device. Radiofrequency energy harvesting is also investigated but it is concluded that this technology is not yet developed for practical use.

Sammanfattning

Genom energiskörd kan produkter bli mer energimässigt självförsörjande vilket ger möjligheten till att slippa dra kabel, förlänga batteritider eller ta bort batterier. I den här uppsatsen undersöks egenskaperna och tillgängligheten hos de mest lovande energiskördsteknologierna. Fokus ligger på mängden potentiell energi tillgänglig och hur begränsad en teknologi är till ett visst område. Olika sätt att lagra och hantera överföring av energi undersöks också.

Två olika energiskördsprototyper presenteras i arbetet. Den första kan skörda ett genomsnitt på 152 mW vid en ljusstyrka mellan 302 och 346 lux med 4 AM-1417 solceller med en area på 19.46 cm^3. Mätningarna sker i lysrörsbelysning i kontorsmiljö. Den andra prototypen skördar energin från en dörröppning med hjälp av en DC-motor. Det är möjligt att skörda mer än 470 µJ från en dörröppning med prototypen. Detta kräver en minsta genomsnittshastighet på 7.5 rpm.

Solceller är relativt enkla att använda i praktiken och en miljö med tillräcklig energi går att finna. Piezoelement och vibrationsbaserad elektromagnetism är svårare att använda generellt eftersom energiomvandlingen bara ger användbara energinivåer vid resonansfrekvensen. Elektromagnetiska tryckknappar och rotationsgeneratorer har däremot visat sig användbara. Termoelektriska element är beroende av speciella miljöer vilket gör dem svåra att använda i flera sammanhang. Radiofrekvensenergiskörd undersöks också men slutsatsen av arbetet är att det inte är tillämpningsbart i praktiken i nuläget.

Preface

This master thesis work has been done at Axis Communications in Lund from the beginning of January to the end of May 2017. The entire project has been performed by the students Oscar Ridell and Pål Nilsson. Although in the testing phase Ridell had a focus on the photovoltaic cells and Nilsson on the DC generator.

We would like to thank Axis Communications and its employees for supporting us with technical knowledge and equipment. We would also like to give a special thanks to our supervisors Mats Larsson and Jonas Sjögren at Axis Communications for always being available for guidance and support. Thanks to Charlotte Gunsjö for supporting and coordinating us through the thesis. Thanks to Jakob Beckerot for assisting us several times with 3D printing. There are many other employees at Axis Communications who has shown a great interest in our thesis and we are grateful for this.

We would also like to thank our supervisor Gunnar Lindstedt and examiner Johan Björnstedt at Lund University Faculty of Engineering Industrial Electrical Engineering and Automation for taking the time to guide us through our thesis and being available for discussions.

Abbreviations

CPU – Central Processing Unit
DMA – Direct Memory Access
EH – Energy Harvesting
EMF – Electromotive Force
EVM – Evaluation Module
FG – Floating Gate
FPGA – Field Programmable Gate Array
IC – Integrated Circuit
I/O – Input/Output
IoT – Internet of Things
MCU – Microcontroller Unit
MPP – Maximum Power Point
MPPC – Maximum Power Point Controller
MPPT – Maximum Power Point Tracking
PoE – Power over Ethernet
PV – Photovoltaic
PVC – Photovoltaic Cell
RAM – Random Access Memory
RF – Radio Frequency
STC – Standard Test Condition
TEG – Thermoelectric Generator
UHF – Ultra High Frequency
WPT – Wireless Power Transfer
WSN – Wireless Sensor Node

Table of Contents

1 Introduction

1.1 Background

The energy consumption of low power products such as sensors keep decreasing. Because of this, the need to power these products through the power grid or batteries is disappearing. An emerging way to power these products is through energy harvesting (EH), also known as energy scavenging. EH is a term that comprises processes where energy is taken from the environment. Some examples of these energy sources are light, heat, kinetic energy and electromagnetic waves [1]. The use of the environment as an energy source enables products to become more self-sufficient of power. From this follows that wiring and battery exchange can be avoided. The product can also become more environmentally friendly and independent of the state of the power grid.

Axis Communications are using Power over Ethernet (PoE) to power their products and are interested in alternative solutions. To get a better insight into the area, Axis requests an evaluation of the different EH technologies, their possibilities and limitations regarding energy collection and practical implementations.

1.2 Problem Statement

This master thesis investigates which EH technologies are available. The most promising and practical technologies are further evaluated. The evaluation includes what amount of potential energy can be harvested with the transducer and how limited the transducer is to a specific environment. Different power management and energy storage methods are also presented and evaluated.

1.3 Goal

The primary goal of the thesis is to gather knowledge about different EH technologies and methods for managing the harvested power. The secondary goal is to build prototypes demonstrating an EH phenomenon.

1.4 Limitations

The master thesis investigates harvesting energy through photovoltaic, thermal, kinetic and electromagnetic transducers. This limitation was decided after a screening of the existing EH technologies. Thereby also recognizing that these were the most practical or popular ones and therefore required further investigation. This thesis does not investigate macro EH like large solar panels or other power plants utilizing for example water flow. Instead, this thesis focus on EH methods relevant for the powering of small systems, often in the µW to mW range. The load of the EH application is not included in the thesis, except for a chapter about low power microcontrollers. This thesis focuses on how to power the load.

2 Method

Literature studies are made to screen the area of EH and investigate which technologies are feasible. The most promising technologies are being further investigated with literature studies. Commercial EH solutions and companies working in the EH field are also investigated. Power management and energy storage methods relevant for EH are investigated through literature studies. Two prototypes are built with the purpose to demonstrate the working principle of EH and to test if it worked reasonably well in an office environment. One of the prototypes is also used to test the difference in performance of two different types of photovoltaic cells.

3 Energy Harvesting

The principle of converting ambient energy into electricity is far developed in technologies like solar panels and wind turbines and can be considered as macro EH. This thesis focuses on micro EH for small scale systems, like ultra-low power devices.

EH means making use of ambient energy which would otherwise be wasted. This energy can come in various types. The type and amount of ambient energy depends on the environment it operates in. These factors also decide which applications are possible. An example of an EH application is a wireless sensor. Powering the sensor with EH allows less frequent battery changes and less cable management.

A figure describing a generic EH application is shown in Figure 1. The application is based on an energy *transducer* which converts the input energy to usable electricity, for example a solar panel converting light into electricity. If the transducer outputs alternate current, a *rectifier* is needed. A *voltage regulator* is needed to control the voltage to a desired level. The optional rectifier and voltage regulator are together denoted *power management*. Lastly, an *energy storage* element might be needed to store the harvested energy. This thesis also defines *EH system* as a transducer together with power management and energy storage. An EH system together with an input energy and a load is called an *EH application*.

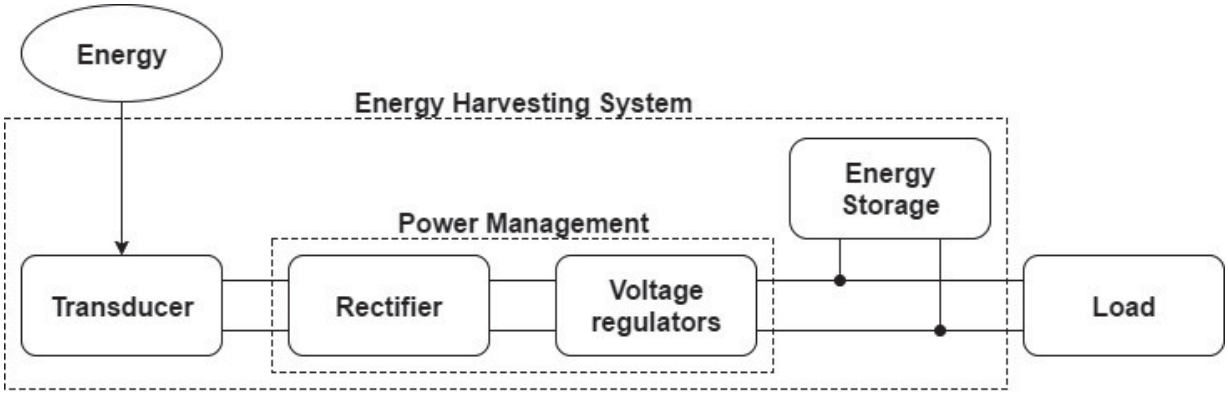

Figure 1. Schematic of a generic EH application.

The amount of harvested energy is often dependent on the volume of the transducer. To fairly compare different EH transducers, the quantity *power density* is used. Power density is often given in power per unit volume or power per unit area. [2]

4 Photovoltaics

The light from the sun reaches earth with a maximum intensity of about 100 mW/cm^2 [2]. Solar panels are becoming more efficient each year. The technique is now so developed solar power can be considered a serious competitor to traditional energy sources. This master thesis focuses on solar panels, or Photovoltaic Cells (PVC), dimensioned for smaller use.

4.1 Photovoltaic Cells

PVCs convert light into electricity. The conversion is achieved through the photovoltaic effect. The photovoltaic effect is closely related to the photoelectric effect. When light shines upon metal atoms, the free electrons can absorb the photons from the light. If the amount of energy in the absorbed photons are high enough, the electrons excites from a lower state to a higher state and may even leave the atom to flow freely. In the photoelectric effect, the electrons flows freely into vacuum space. In the photovoltaic effect, the freed electrons jumps directly to another material and not into a vacuum space.

The excitation of an electron by absorption of a photon creates a positive charge called a hole. That is, the absorption of a photon separates an electron from a hole. The electrons and holes are moved with an electric field to their respective electrodes. By offering an external path the electron-hole pair can reunite. By constantly exploiting this effect, a current is created [2] [3].

Figure 2 shows a model of a simple PVC with 3 active layers:

- The top layer is a top junction layer which is made of an n-type semiconductor.
- An absorber layer, which is made of a p-n junction.
- A back junction layer, which is made of a p-type semiconductor.

The P-N junction creates the electric field in the cell. The electric field provides the voltage needed to force the electrons and holes, which have been freed by the absorption of photons, to flow in the right directions. The electrons flow to the n-type side and the holes to the p-type side. An external current path is provided through which the electrons can flow back and unite with the holes. The electrons flowing provides the current and the cell's electric field provides the voltage. The process is illustrated in Figure 2 [4].

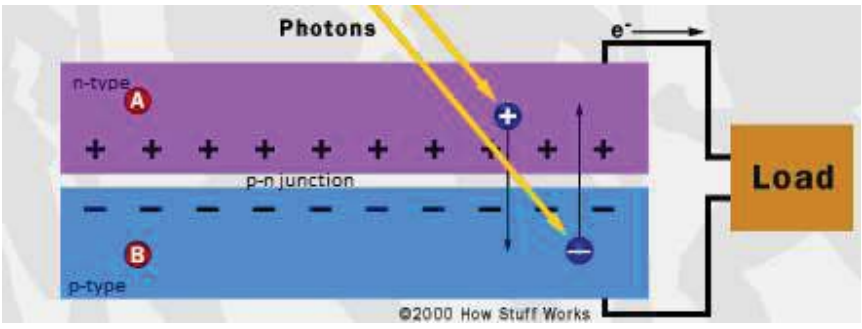

Figure 2. The working principle of a PVC. The purple side (A) is an n-type semiconductor and the blue side (B) is a p-type semiconductor [4].

4.2 Efficiency

4.2.1 Factors lowering the efficiency of PVCs

PVCs generally have a low energy conversion efficiency. Factors lowering the efficiency can be grouped into four categories [3]:

- Some photons that hit the cell may be reflected by the cells surface. They may also hit the metal grid used for mounting the cells.
- Not all photons have sufficient energy to be absorbed by the cell while some photons have too much energy. Photons with too much energy create electron-hole pairs, but the surplus energy is in form of heat which splits the electron from the nucleus.
- An electron-hole pair may on the journey towards the electrodes meet opposite charges and recombine.
- The efficiency is also lowered because of different types of parasitic resistance. For example, there are metallic contacts that collects the charges from the depletion region that are placed in the front and back of the cell. These contacts have a certain amount of resistance which lowers the power transferred to the load.

4.2.2 Theory

The maximum voltage given from a PVC ranges up to the open circuit voltage, V_{oc}. V_{oc} is the voltage given when the PVC is not connected to anything. The maximum current produced by the PVC is the short circuit current, I_{sc}. The current produced is approximately proportional to the illuminated area of the PVC, therefore the quantity short circuit current density, J_{sc}, is used. This is also motivated by the fact that when comparing EH devices, power density is often used.

A PVCs power density is given by

$$P = J * U$$

where J is the current density and U is the voltage. The power density reaches its maximum at the maximum power point, at a voltage V_m and a current density J_m. A fill factor, FF, is introduced to describe the ratio between the maximum output power density and the theoretical maximum output density.

$$FF = \frac{J_m * V_m}{J_{sc} * V_{oc}} = \frac{Real\ maximum\ output\ power\ density}{Theoretical\ maximum\ output\ power\ density}$$

A current density-voltage curve, JV curve, of an arbitrary PVC, is shown in Figure 3 below. The maximum power density is given by the area of the inner rectangle. The theoretical maximum power density is given by the outer rectangle. If the fill factor was equal to 1, the JV curve would follow the outer rectangle. The grey line is the power density. It can be seen that it reaches its maximum at the maximum power point.

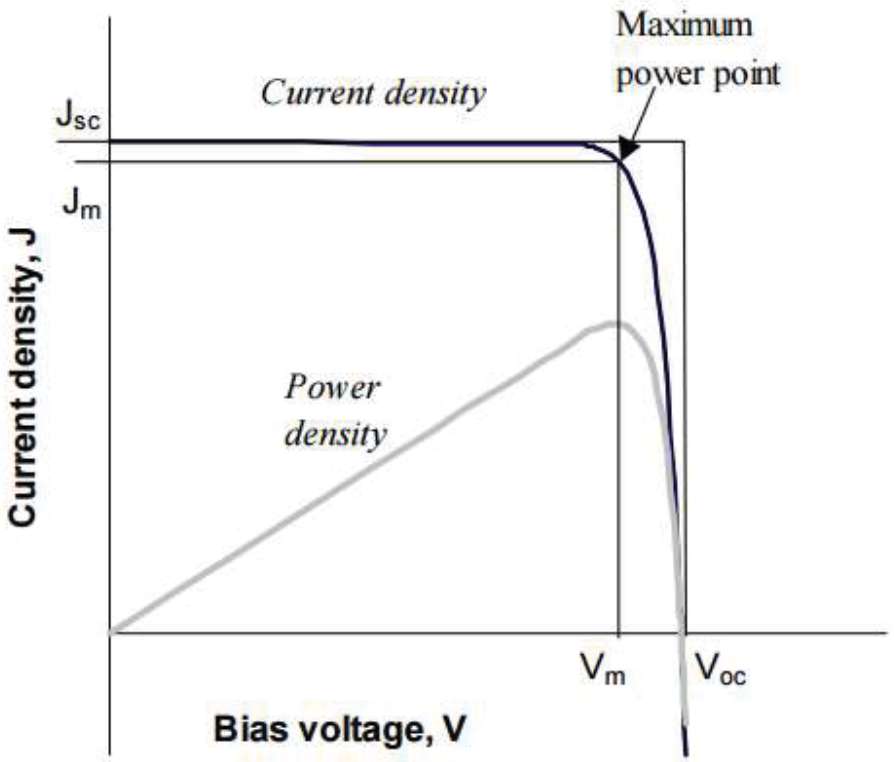

Figure 3. JV curve of an arbitrary PVC [5].

The efficiency, η, of the PVC is the power density delivered at the maximum power point divided by the input power, P_s.

$$\eta = \frac{J_m * V_m}{P_s}$$

It can also be expressed in terms of

$$\eta = \frac{J_{sc} * V_{oc} * FF}{P_s}$$

The four quantities J_{sc}, V_{oc}, FF and η are the key performance characteristics of a PVC. They should be defined for particular illumination conditions. For example, the Standard Test Condition (STC) for PVCs is the Air Mass 1.5 spectrum, input power density of 1000 W/m^2 (1 sun) and a temperature of 25 degree C [5].

4.2.3 Temperatures effect on efficiency

The performance of a PVC varies with temperature. PVCs have a higher efficiency in cold temperatures and a lower efficiency in warm temperatures. To show how the cells performance varies with temperature, the unit $\Delta W/K$ or similar is used. It is given at STC. It shows how the output power increases if the temperature drops below 25 ℃ or decreases if the temperature rises above 25 ℃. The manufacturer may choose to present the temperature coefficient for voltage and current separately instead.

To get an idea of how much the efficiency can vary with temperature an example is given from the Panasonics Amorton series [6] where the PVCs has the temperature coefficients:

$$V_{oc} = -0.45\%/℃$$

$$I_{sc} = +0.08\%/℃$$

4.2.4 Maximum Power Point Tracking

A PVCs output current and voltage varies with ambient conditions, for example illumination and temperature. This results in a variation in output power. To account for this variation and to always output the maximum amount of power, Maximum Power Point Tracking (MPPT) is used. Maximum Power Point Controllers (MPPC) controls the input voltage by acting as a variable load to make sure that the input power is as close to the maximum power point in the JV curve as possible. Typically, PVCs have their maximum power point at 80% of the open circuit voltage [7].

MPPT is not only used in PVC applications, but in other high impedance applications as well. For more information about MPPT, see chapter about Maximum Power Point Tracking.

Figure 4 shows JV curves for a SANYO HIT 215W solar panel at different illuminances. It illustrates how the maximum power point can vary with illumination. Observe that this is a large solar panel and not a small PVC, but the principle is the same.

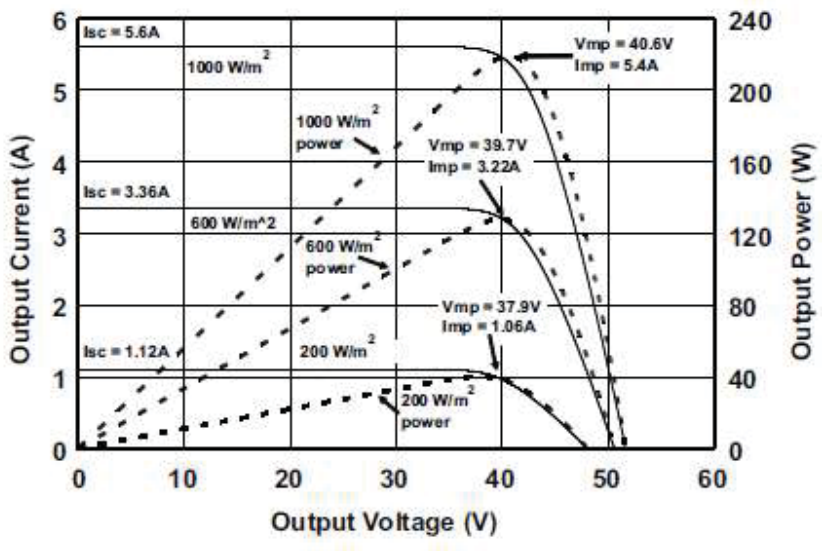

Figure 4. JV-curves and power density at different illuminances for SANYO HIT 215W, demonstrated by Dave Freeman in Introduction to Photovoltaic Systems Maximum Power Point Tracking [8].

4.3 Types of Photovoltaic Cells

There are different types of PVCs. The majority of them are based on silicon. The most common are monocrystalline, polycrystalline and amorphous cells. These have different efficiencies and spectral range.

4.3.1 Monocrystalline

Monocrystalline cells are made of monocrystalline silicon. They have the highest efficiency rate and are the most expensive [9]. The efficiency varies between manufacturers but they are usually about 14-22% [10] [11]. Some have a reported efficiency of up to 26.3+-0.5 % [12]. The high efficiency rate makes them the most space-effective choice.

4.3.2 Polycrystalline

The process of producing polycrystalline silicon cells is simpler and cheaper, compared to the monocrystalline cells. The amount of waste silicon is also less. Polycrystalline cells have an efficiency of about 13-16% [9], but some have a reported efficiency of up to 21.3+-0.4 % [12]. The lower efficiency, compared to monocrystalline cells, requires larger volumes to produce the same amount of energy.

4.3.3 Amorphous

Amorphous cells use about 1% of the amount of silicon used in crystalline cells [9]. They have a much lower efficiency compared to mono and polycrystalline cells. The efficiency is about 5-8% [10] [11], but some have been reported to have an efficiency up to 10.2+-0.3% [12]. Amorphous cells are mostly used in low power devices like pocket calculators. Amorphous cells show promise since they require much less silicon, can be made out of inexpensive materials such as glass, stainless steel and plastic and they tolerate heat pretty well [11].

4.3.4 Thin-Film

Thin-film photovoltaic cells can be made of different kind of materials, for example amorphous silicon, Cadmium telluride, Copper indium gallium selenide and organic PVCs. They have lower efficiency compared to mono and polycrystalline cells. It is about 7-13%. An advantage is that the thin-film PVCs can be made flexible. Generally, thin-film PVCs are cheap but requires a lot of space due to their low efficiency [9].

4.4 Illumination and Light Spectrums

4.4.1 Lux

The output power of a PVC increases with increased illumination. The illumination is measured in lux which is the amount of illuminance per square meter. The illuminance is measured in lumen [lm]. Lumen measures the light flux emitted from a source.

The Swedish Work Environment Authority offers recommendations for lux values in different environments. These are given in Table 1 [13]. These values can be compared with the performance of PVCs at different lux values to determine how well the PVCs are suited for different environments.

Table 1. Recommended lux values in different environments from the Swedish Work Environment Authority [13].

Place/Working function	**General lighting (lux)**	**Spotlighting (lux)**
Archiving, copying	200	300
Normal work in the office	300	500
Working stations for CAD	300	500
Work with a higher demand on seeing	300	750
Finer drawing	500	1500
Conference room	200	500
Cleaning	Minimum 200 lux on the floor	
Garbage room	100	

4.4.2 Light Spectrums

Indoor PVCs are optimized for poor light conditions while conventional outdoor solar panels are more efficient in high outdoor illuminances. White LED light is the latest trend in indoor light and it is fast-growing and promising. Through different selection of compounds and ion changes, coated LED lamps can imitate multiple user specific light demands. According to EnOcean [14], the amorphous PVCs show similar efficiency under all evaluated indoor illumination sources (incandescent, compact fluorescent lamp and white LED) and is according to them the overall optimal light harvester solution for typical indoor light conditions.

Figure 5 shows that the spectral sensitivity of the amorphous PVC (a-Si) overlaps that of the human eye, which means that every light source provided for human use matches the a-Si cell too. According to both EnOcean [14] and IXYS [11] amorphous cells works best in indoor light, while monocrystalline and polycrystalline works best in outdoor light. This is also illustrated in Figure 5, where it is shown that amorphous cells work best in the 400-700 nm interval, which corresponds to the light visible to our eyes, and the crystalline cells (c-si) in the 600 nm to 1000 nm interval.

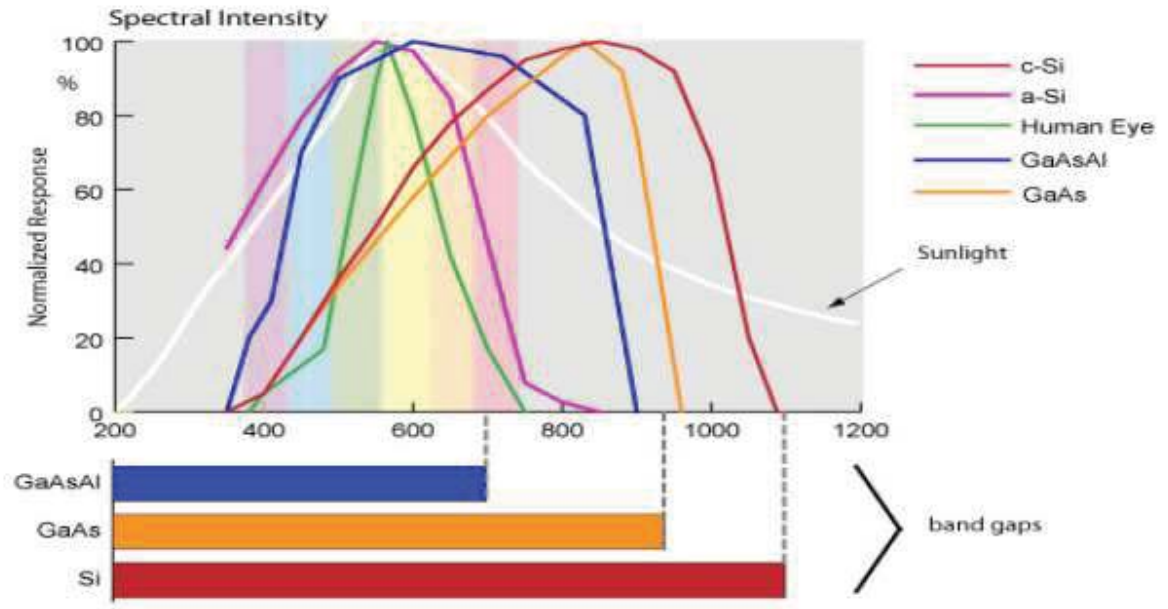

Figure 5. Normalized response of different PVC techniques with respect to light spectrum. The x-axis is given in nanometers. [14]

Figure 6 from EnOcean [14] shows the wavelengths of different light sources and their relative energy.

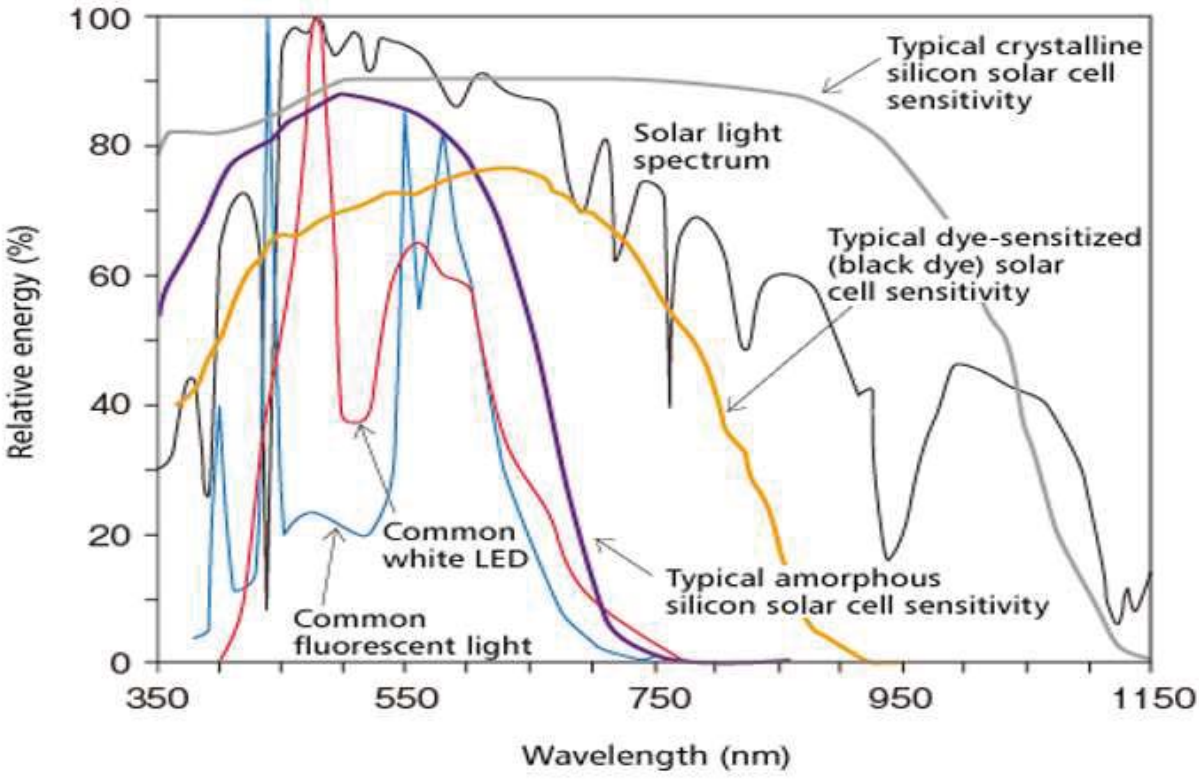

Figure 6. Relative energy in different wavelengths from different light sources [14].

5 Piezoelectricity

5.1 Energy Conversion

Mechanical energy can be harvested through vibrations or strains with the piezoelectric effect. The piezoelectric effect occurs in crystals with no center of symmetry. Under normal conditions, the positive and negative charges in the crystal are separated but symmetrically distributed. The symmetry is destroyed when the crystal is exposed to strains. The asymmetry created when straining the crystal generates a voltage. Piezoelectric materials also show the reverse piezoelectric effect, that is, the crystal will deform when it is exposed to a voltage [15]. Other transducers converting mechanical energy to electricity are inductive- and electrostatic transducers. Piezoelectric transducers have a higher power density than these [15] [16] [17], but are not entirely easy to use. The piezoelectric transducers potentially high power density occurs when they vibrate at their resonance frequency. This means that the frequency of the harvested energy has to be close to the resonance frequency of the transducer. Cantilever beam structures are often utilized to construct a transducer with a specific resonance frequency to customize it to the intended environment [18].

5.2 Vibrations

A vibration is characterized by its frequency and peak acceleration. Different potential vibration sources are summarized by Kin et al. [18] and are shown in Table 2.

Table 2. Different vibration sources.

Human Body	Vehicles	Structures	Industrial	Environment
Walking, arm motion, finger motion, jogging, swimming, eating, talking	Aircraft, unmanned air vehicle, helicopter, automobiles, trains	Bridges, roads, tunnels, farm house structures	Motors, compressors, chillers, pumps, fans	Wind, solar, temperature gradient, daily temperature
Breathing, blood pressure, exhalation, body heat	Tires, tracks, peddles, brakes, shock absorbers, turbines	Control switch, heating ventilation and air conditioning systems, ducts, cleaners, etc.	Conveyors, cutting and dicing, vibrating machine	Ocean currents, acoustic waves, electromagnetic waves, radio frequency signal

The two rows in this table represent the difference in the scale of the mechanical energy.

Roundy [17] concluded that most ambient vibration sources have relatively low frequencies, below 200 Hz, with widely varying acceleration levels. Some peak accelerations and frequencies of common structures found in typical office buildings, homes or manufacturing plants are summarized by Roundy and shown in Table 3.

Table 3. Frequencies and accelerations of common structures found in typical office buildings, homes or manufacturing plants.

Vibration Source	Peak Acc. (m/s^2)	Frequency of Peak (Hz)
Base of 5 HP 3-axis machine tool with 36" bed	10	70
Kitchen blender casing	6.4	121
Clothes dryer	3.5	121
Door frame just after door closes	3	125
Small microwave oven	2.25	121
HVAC vents in office building	0.2 – 1.5	60
Wooden deck with people walking	1.3	385
Breadmaker	1.03	121
External windows (size 2 ft X 3 ft) next to a busy street	0.7	100
Notebook computer while CD is being read	0.6	75
Washing Machine	0.5	109
Second story floor of a wood frame office building	0.2	100
Refrigerator	0.1	240

5.3 Piezoelectric Materials

An obvious distinction between piezoelectric materials is the stiffness of the actuators. Soft piezoelectric crystals show larger strains than hard ones at a given load, but is more prone to depolarize. However, the brittle variations of piezoelectric materials run a risk of fractures due to crack propagation. According to Spies et al. [2], the maximum tensile stress of a piezoelectric bulk material is 10 MPa and the maximum compressive stress is typically 10 times greater.

When a piezoelectric material is heated up to its Curie temperature, the crystal becomes symmetric and depolarizes. This makes it unable to generate a voltage. For PZT, which is the most common piezoelectric material, the Curie temperature varies between 250 and 400 ℃, depending on its composition.

A selection of common piezoelectric materials are summarized in Table 4. The data is taken from Spies et al [2].

Table 4. The most common piezoelectric material and their properties.

Piezoelectric material	**Density (g/cm^3)**	**Curie Temperature (℃)**
Quartz	2.65	537 (phase transition)
$BaTiO_3$	5.85	120
PZT 4	7.9	328
PVDF-TrFE	1.8	102
1-3 Piezo	3	328

5.4 Examples of Piezoelectric Transducers

Kin et al. [18] believes that in the near future, a coin-sized harvester will be able to harvest about 100 µW of continuous power below 100 Hz at less than 0.5 g vibration at reasonable cost. However, there are almost no commercial solutions in the market today. Roundy constructed some customized piezoelectric transducers used to power Wireless Sensor Nodes (WSN) [17], these are summarized in Table 5. The designs are shown in Figure 7, Figure 8 and Figure 9.

Table 5. Piezoelectric transducers created by Roundy.

Design	Maximum Output Power (μW)	Volume (cm^3)	Power Density (μW/cm^3)	Frequency (Hz)	Acceleration (m/s^2)
1	207	1	207	85	2.25
2	335	1	335	60	2.25
3	1700	4,8	354	40	2.25

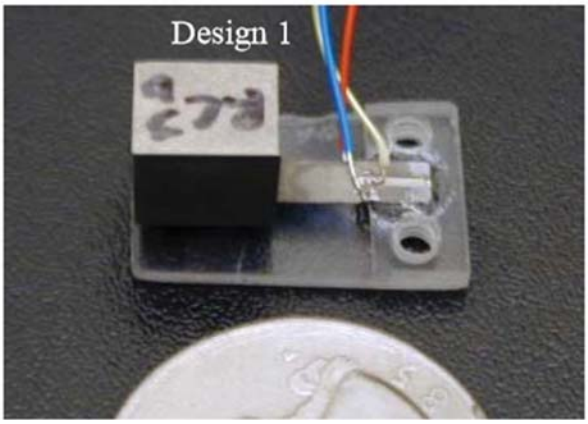

Figure 7. Piezoelectric transducer, design 1 [17].

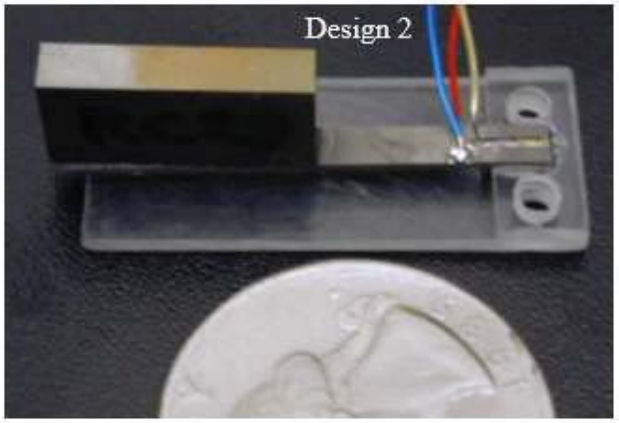

Figure 8. Piezoelectric transducer, design 2 [17].

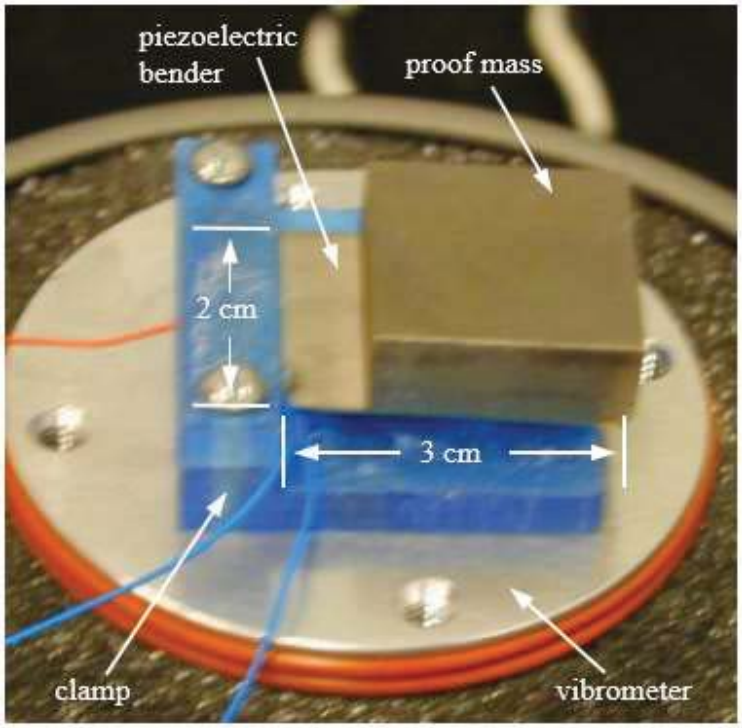

Figure 9. Piezoelectric transducer, design 3 [17].

Kin et al. [18] summarizes some recent piezoelectric energy harvesters, show in Table 6. They are much smaller compared to Roundy, Table 5.

Table 6. Table of recent piezoelectric energy harvesters.

Reference	Active Material	Active Area, mm²	Active Volume, mm³	Acceleration, g	Frequency, Hz	Power, μW	Power Density, μW/mm³
Muralt 2009[25]	PZT, d_{33}	0.96	0.48	2.0	870	1.4	7.78
Morimoto 2010[13]	PZT, d_{31}	92.5	0.26	0.5	126	5.3	20.5
Hajati 2010[19]	PZT, d_{33}	120	0.02	4.0	1300	22	1100.0
Durou 2010[28]	PZT	9.45	1.89	0.2	76	13.9	7.35
Defosseux 2011[30]	AlN, d_{31}	3.573 (est.)	2.8	0.275	214	0.63	0.23
Marzencki2008[31]	AlN, d_{31} (vac.)	1.573 (est.)	–	0.126	214	0.55	–
Hirasawa 2010[32]	AlN	–	1.63	1.0	857	0.18	0.110
Elfrink 2010[38]	AlN	–	15	0.2	599	69	4.60
Xu 2011[39]	PZT	–	20.9	1.0	329	7.35	0.35
Lei 2011[40]	PZT	–	18.6	1.0	235	14	0.75
Park 2010[41]	PZT, d_{33}	1.8	1.05	0.39	528	1.1	1.05
Fang 2006[42]	PZT, d_{31}	2.65	0.78	1.0	608	2.16	2.77
Aktakka 2011[45]	PZT, d_{31}	49	27	1.5	154	205	7.59
Kanno 2012[76]	KNN, d_{31}	56.1	0.168	1.0	1036	1.1	6.54

5.5 Piezoelectric Transducer Characteristics in Low Frequencies

Low frequency piezoelectric transducers can be described as a capacitor parallel coupled to a charge source. The energy stored can be described by the energy equation for a capacitor.

$$E = \frac{1}{2} * C * U^2$$

The equation shows that it is beneficial to allow the voltage to peak before extracting the energy. Given the same peak loading force, the charge generated for each cycle is relatively constant, regardless of frequency. Low frequency piezoelectric transducers outputs high voltage but very low current [19].

Researchers at the MIT Media Lab, Shenck and Paradiso [19], demonstrated two different approaches of harvesting the kinetic energy that comes from walking using piezoelectric transducers. One approach, implemented in a pair of sneakers, was able to harvest an average power of 1.3 mW when walking at 0.9 Hz. This method harvested the energy dissipated when bending the ball of the foot, using the piezoelectric material Polyvinylidene Fluoride (PVDF). The other approach, implemented in a US Navy work boot, using the piezoelectric material PZT, was able to harvest an average power of 8.4 mW under similar conditions. This method harvested the energy that comes from the heel strike when walking. The feasibility and utility of the prototypes where proven by the powering of an active radio frequency tag that transmitted a short-range, 12-bit wireless identification code while the bearer walked. This system was completely self-powered by the piezoelectric energy harvester. The two prototypes produced high-voltage, low-energy, low current pulses at about 1 Hz, when walking. This resulted in extremely high source impedance, giving voltage signals in the 100 V range and currents in the 10^{-7} A range. To account

for this, Shenck and Paradiso designed a customized converter since they assessed that the commercial available ICs were inappropriate for these special circumstances.

5.6 Theoretical Model

Shu et al. [20] derives a piezoelectric EH model thoroughly. A brief recap is explained here. A piezoelectric generator, consisting of a vibrating piezoelectric structure and an energy storage system, can be described as a mass + spring + damper + piezo structure, se Figure 10.

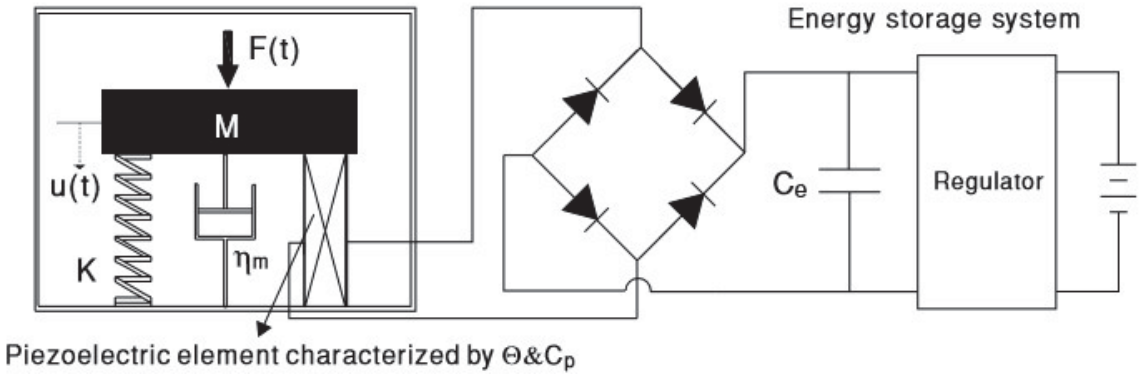

Figure 10. Model of a piezoelectric generator.

The piezoelectric element is coupled to a mechanical structure. The mechanical structure is characterized by a mass, M, a spring coefficient, K, and a damping coefficient, η_m. The piezoelectric element is characterized by the effective piezoelectric coefficient, Θ, and capacitance, C_p. These constants depend on the geometry and material of the transducer and the load direction.

An excitation function $F(t)$ is applied to the system. The displacement of the mass, M, is denoted u and the voltage across the piezoelectric element V_p. The equations for the vibrating structure, consisting of the mechanical structure and the piezoelectric element, can be described by

$$M\ddot{u}(t) + \eta_m\dot{u}(t) + Ku(t) + \Theta V_p(t) = F(t)$$

$$-\Theta\dot{u}(t) + C_p\dot{V}_p(t) = -I(t)$$

where $I(t)$ is the current flowing into the circuit. Most forces applied on a piezoelectric material when the purpose is power generation should be vibrations and can be described as a periodic force. The piezoelectric structure is therefore assumed to be driven at a frequency around resonance with the force

$$F(t) = F_0\sin(\varpi t)$$

where the constant force magnitude is denoted F_0 and the angular frequency of vibration ϖ, given in radians per second.

5.7 Future and Challenges

Piezoelectricity have been thoroughly investigated since the late 1990s. It is still an emerging technology. To make piezoelectric transducers more convenient, new configuration approaches and operating modes are under development. The aim is often to create broad bandwidth harvesters that are able to harvest energy from different environments. To make piezoelectric harvesters more environmentally

friendly, new materials are being investigated. [18]

An interesting area is nanoscale harvesters. This is still an emerging technique in its early stage and requires further research. [15]

Frequency tuning methods and non-resonant solutions are methods which can be used to improve piezoelectric generators. However, these methods come at an expensive energy cost and may not be applicable in low energy application. [15]

6 Electromagnetism

6.1 Energy Conversion

An electromagnetic generator, or induction generator, works by converting mechanical energy into electrical energy by the induction of an Electromagnetic Force (EMF). This principle is described by Faraday's law. If a permanent magnet moves relative to a coil, it creates a change in the electromagnetic flux through the coil. This causes an EMF, or voltage, to be generated in the coil. The induced voltage generates a current. The flux variation is the key factor and it can be done with a moving magnet and a fixed coil or with a fixed magnet and a moving coil. The first configuration is often the best since this allows the electrical wires to be fixed. The induced voltage is dependent on the number of turns in the coil and the time derivate of the magnetic flux. This means that larger transducers with longer copper wires and more turns will perform better than small ones, unless large velocities are involved. This is a problem for small scale EH systems [2].

The relative motion of a permanent magnet and a coil can be created by vibrational or rotational movement. A vibration generator has to vibrate around its resonance frequency to output a useful amount of power. A rotation generator's output power increases with an increasing speed.

The electromagnetic transducers output power performance is strongly dependent on the design of the electromagnetic coupling. Size, material properties and geometric configuration of magnets, coil and magnetic circuits are determining factors.

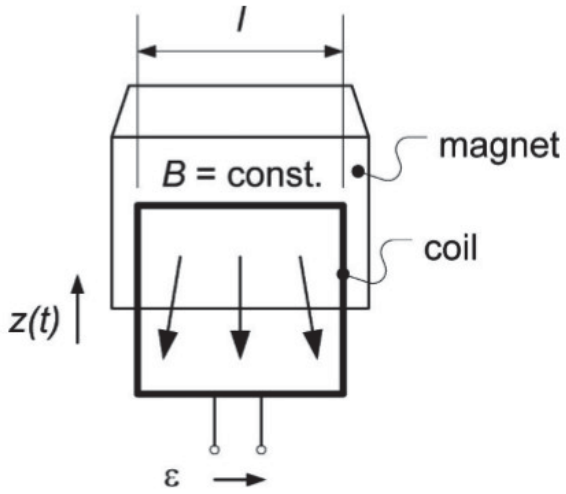

Figure 11. Model of a basic electromagnetic transducer, as proposed by Spies et al. [2].

Faradays law describes how electromagnetism works. The law says that in a closed circuit in a time-varying magnetic field, a voltage, a.k.a. EMF, is induced. The magnitude of the voltage is equal to the time derivative of the magnetic flux. The magnetic flux, φ, is described by

$$\varphi = \iint_A BdA$$

where B is the magnetic flux density and A is the area enclosed by the wire loop, as shown in Figure 11. The induced voltage, ε, is given by

$$\varepsilon = -\frac{d\varphi}{dt} = -\left(\frac{dA}{dt} * B + \frac{dB}{dt} * A\right)$$

This equation offers a wide range of implementations of the electromagnetic coupling, since it does not matter if the magnetic field is changing during a constant area or if the area is changing during a constant magnetic field. For a coil of wire with N identical turns, Faradays law of induction states

$$\varepsilon = -N * \frac{d\varphi}{dt} = -N * \left(\frac{dA}{dt} * B + \frac{dB}{dt} * A\right)$$

where N is the number of turns of wire and φ is the magnetic flux through a single loop. The equation is often simplified, assuming constant $\frac{dB}{dt}$, to ease the calculations.

$$\varepsilon = -N * B * \frac{dA}{dt} = -N * B * I * \dot{z}$$

A model of an electromagnetic vibration transducer is shown in Figure 12.

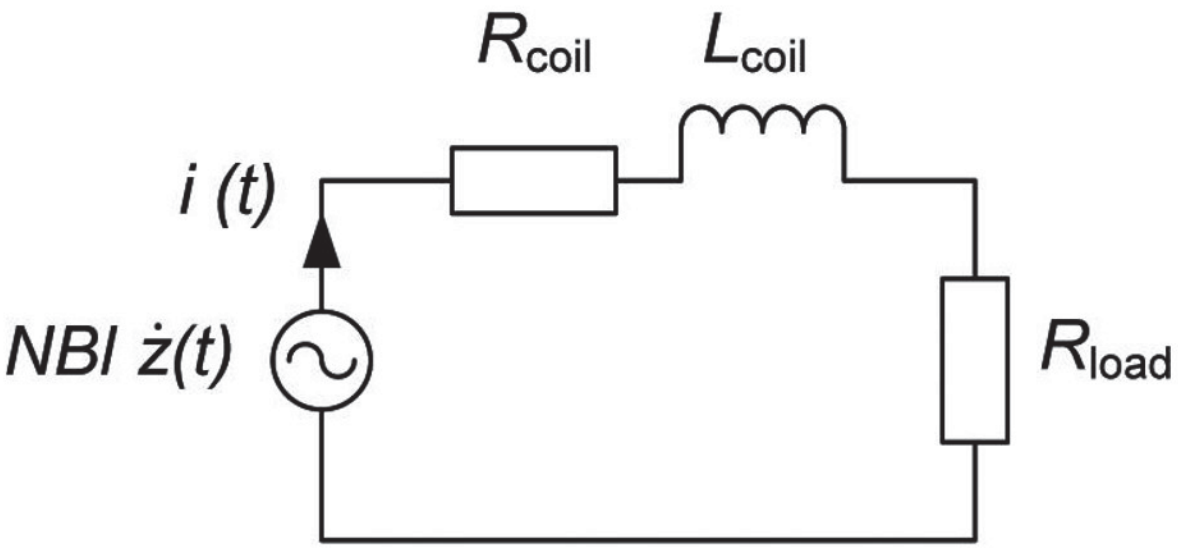

Figure 12. Electrical model of an electromagnetic vibration transducer [2].

The governing equation is

$$L_{coil} * \dot{i}(t) + (R_{coil} + R_{load}) * i(t) = -N * B * l * \dot{z}(t)$$

where $u = L_{coil} * \dot{i}(t)$ is the voltage over the coil [2].

To calculate the expected output power of a DC motor a number of equations are used. The different variables used when calculating the expected output power are the stall current, I_{stall}, the no-load speed in rpm, n_{NL}, the no-load current, I_{NL}, and the terminal voltage, V_t. The stall current is the motor current when the shaft is fixed. The no-load current is the motor current when there is nothing

connected to the shaft. The no-load speed is the motor speed when nothing is connected to the shaft. To arrive at an output power, these attributes have to be inserted into a series of equations.

Armature resistance is given trough the ratio between the terminal voltage and the stall current.

$$R_a = \frac{V_t}{I_{stall}}$$

From the armature resistance, the no-load induced armature voltage can be calculated.

$$E_{a,NL} = V_t - I_{NL} \cdot R_a$$

This can be used to calculate the motor constant.

$$k = \frac{E_{a,NL}}{n_{NL}}$$

The motor constant combined with the actual speed of the shaft gives the induced armature voltage.

$$E_a = k \cdot n$$

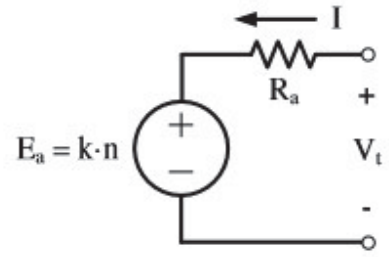

Figure 13. Model of a DC motor.

To calculate the maximum output power of a DC motor, the maximum power transfer equation, or Jacobis Law, is used. It is based on the fact that the output power reaches its maximum when the load resistance, R_l, is equal to the power source resistance, R_s, when R_s is constant. Figure 14 is used to derive the maximum power transfer equation.

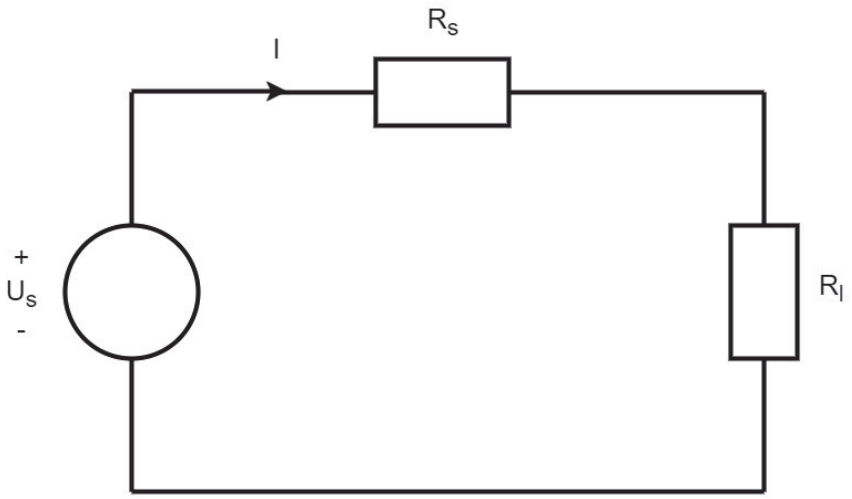

Figure 14. Circuit of a power source, source resistance and load resistance.

$$P_l = U_l * I = R_l * I^2 = R_l * \left(\frac{U_s}{R_s + R_l}\right)^2 = \frac{{U_s}^2}{\frac{{R_s}^2}{R_l} + 2 * R_s + R_l}$$

P_l reaches its maximum when $R_l = R_s$. This gives:

$$P_{l,max} = \frac{{U_s}^2}{4R_s}$$

In the case with the DC-motor, $U_s = E_a$ and $R_s = R_a$, giving

$$P_{l,max} = \frac{E_a^2}{4R_a}$$

6.2 Vibration Generators

The chapter Vibrations under Piezoelectricity explains the phenomenon of vibrations and presents different vibration sources. The vibrations can be harvested by means of inertia based spring-mass systems, where the transducer is customized to resonate at the frequency of the mechanical input source. This way, the energy obtained is maximized. The problem with using these kinds of transducers in small scale EH devices is that as the transducer becomes smaller, the resonance frequency increases and becomes much higher than the characteristic frequencies of many everyday mechanical stimuli. Spies et al. summarizes some vibration generators customized for different frequencies, shown in Table 7 [2].

Table 7. Summary of different vibration generators customized for different frequencies.

Design author	Mechanical excitation	Output power	Dimensions
Williams et al.	$f = 4$ kHz Amplitude = 300 nm	0.3 μW	mm^3
Li et al.	$f = 64$ Hz Amplitude = 1000 μm	10 μW @ 2 V	1 cm^3
Ching et al.	$f = 104$ Hz Amplitude = 190 μm	5 μW	—
Amirtharajah et al.	$f = 2$ Hz Amplitude = 2 cm	400 μW @ 180 mV	—
Yuen et al.	$f = 80$ Hz Amplitude = 250 μm	120 μW @ 900 μV	2.3 cm^3

6.2.1 MEMS Vibration Generators

Pan et al. [21] brings up some examples of Micro Electromechanical Systems (MEMS) vibration generators. Figure 15 shows an MEMS vibration generator consisting of a vibration spring, a copper coil and a permanent magnet of neodymium-iron-boron. The volume of the generator is 240 mm^3 and the weight is 500 mg. It operates at resonant frequency of 322 Hz and an amplitude of 25 μm. Its root-mean-square voltage output is 12.8 mV and its average power output is 530 μW, with a loading resistor of 0.28 Ohm at 322 Hz [22].

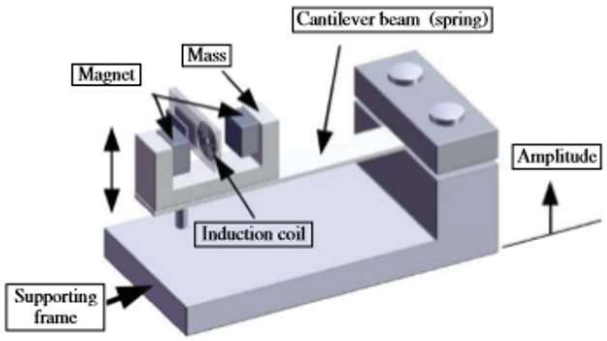

Figure 15. MEMS vibration generator with a maximum power output of 53 μW and a volume of 240 mm^3 [21].

Another example is a tubular MEMS vibration generator, shown in Figure 16. The generator consists of a cylindrical spiral spring, a mass with an induction coil and a permanent magnet. The vibration mass weighs approximately 500 mg. Vibrations with an amplitude of 20 mm and frequency of 100 Hz were able to induce a voltage of 0.18 V and power output of 400 μW.

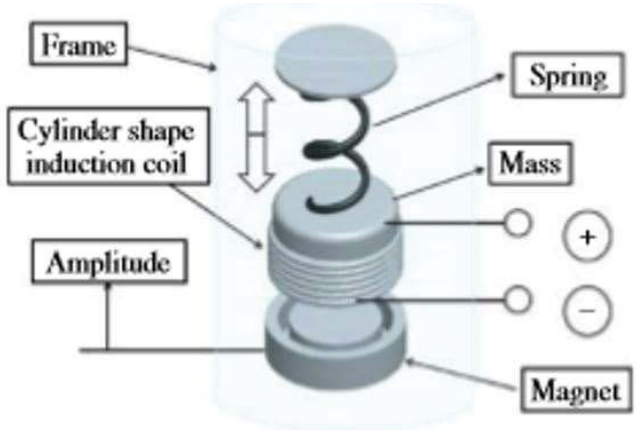

Figure 16. MEMS tubular vibration micro generator with a power output of 400 µW [21].

6.2.2 Pushbutton Generators

A working commercial example of a pushbutton generator is EnOceans Energy Converter ECO 200 [23], shown in Figure 17 and Figure 18. It consists of a magnet, two magnetically conductive laminations, a U-core and a coil. The coil is wrapped around the U-core and the magnetic parts are held in position by a plastic frame and a spring-loaded clamp. The U-core is movable and can take two positions. Each position touches the opposite magnetic poles. In each end position of the U-core, the magnetic flux is reversed. This design enables high magnetic flux alteration with minimal movement of the core, which results in a high efficiency. The power output from the converter is approximately always the same, thanks to a leaf spring which stores the external force applied to the converter. As the leaf spring is bent, it stores more mechanical energy until the magnetic forces no longer are able hold the U-core in its position. The holding force, of about 3.5 N, is exceeded and the core flips into its other position, accelerated by the spring. This generates a voltage pulse in the induction coil. Since the spring always will accelerate the U-core in a similar way, irrespective of how fast it was tensioned, the flipping speed will always be similar. This makes the power output from the converter repeatable and approximately the same each time it is actuated [24].

The energy output from the ECO 200 lies between 120 to 210 µJ at 2 V and its dimensions are 29.3 x 19.5 x 7.0 mm. The ECO 200 can power the PTM 330 radio module and each actuation gives sufficient power to transmit a signal [23]. A drawing of ECO 200 is shown in Figure 17 and the real product is shown in Figure 18.

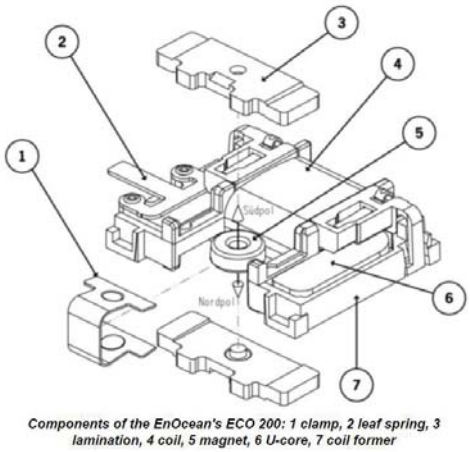

Figure 17. A drawing of the ECO 200, presented by Frank Schmidt [24].

Figure 18. The ECO 200, presented by Schmidt [24].

6.3 Rotation Generators

The key factor to getting high power from rotation generators is the rotation speed. A high speed results in a high time derivative of the flux, which means a high induced voltage. The high speed can be achieved with a gearing system, but a higher gearing also means that more torque is needed to turn it. An electromechanical motor, like a DC motor, can be used as a generator, by rotating the shaft while applying torque to it.

Litwhiler and Gavigan [25] managed to power the locking mechanism of an electronic door lock controlled by card swipes, with a DC generator. The energy required was about 0.8 J. The converter consisted of the DC motor as a generator, a rectifier bridge, a boost converter to raise the voltage from approximately 3.4 V to 9 V and supercapacitors as energy storage. A fixed frequency of 10 kHz was obtained from a function generator and used to drive the boost converter. The schematic of the converter is shown in Figure 19.

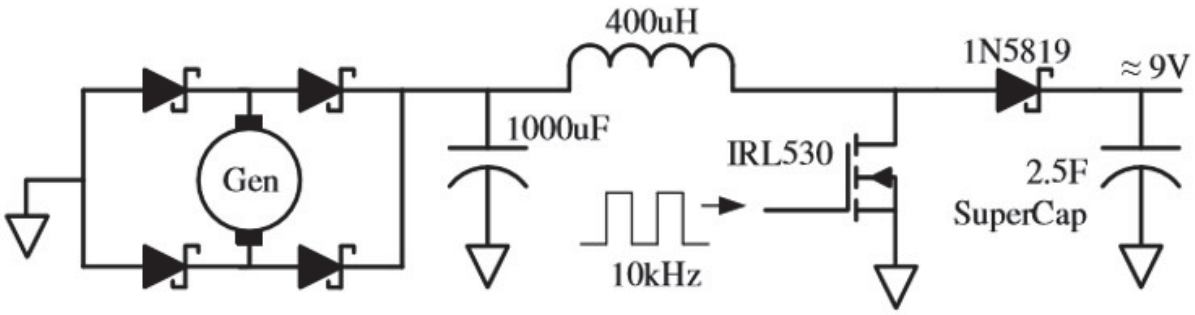

Figure 19. Electric schematic of the door motion energy harvester.

Litwhiler and Gavigan used a DC motor with a maximum output power of 0.53 W.

7 Radio Frequency

Radio Frequency (RF) EH transduces energy from electromagnetic fields in frequencies above 30 kHz [2]. In this chapter, RF harvesting from the Ultra-High Frequency (UHF) span in the far-field region will be investigated. UHF is the span between 30MHz to 3GHz. Signals sent in the UHF band are found in most places in domesticized areas today [26]. The far-field region is where the ratio of the distance, from sink to source of the magnetic field, to the transmission wavelength is much greater than one [2].

To pick up and convert the signals being sent in the UHF span, an antenna is needed. Since the current is alternating, a rectifier is also needed. A combined antenna and Schottky diode is called a rectenna and is usually used in RF EH. When designing an RF harvester, the rectenna should be tuned to the same frequency band as where the signals in the area of implementation are. Since it is not possible to make an antenna able to pick up signals over the entire UHF band, only a part of the band can be harvested with one antenna.

The voltage induced in the circuit when harvesting RF is relatively low which means it will have to be converted to usable levels. This is often done with a charge pump since the voltage might be too low to be usable even by most voltage converters [27]. The harvestable power from RF harvesting is also lower than most other EH methods. When transmitting power in the far-field, there will be losses proportional to the distance of the source squared. In a domestic setting, an antenna can pick up power levels in the range of some picowatts per cm^2 antenna from ambient radio signals [26].

Research is being done in the Wireless Power Transfer (WPT) field with the hopes of making wireless chargers and powering Internet of Things (IoT) units without using batteries or cables. Since RF harvesting is a part of this field, advances might be done in the future. At the moment the power levels of the signals are too low to be feasible in EH systems. There is also regulations on the amount of power a radio transceiver is allowed to radiate which is limiting the practicality of RF harvesting and WPT.

8 Thermoelectric generator

8.1 Energy Conversion

Thermal energy is described by a temperature gradient and a heat flow. Thermoelectric Generators (TEG) converts thermal energy into electrical energy. TEGs are based on the Seebeck effect. The Seebeck effect states that two conductors connected in series with different temperatures will cause a potential difference between them. The potential difference occurs because of the temperature gradient between the conductors. The temperature gradient results in the charge carriers at the hot end getting a high kinetic energy and therefore diffusing to the cold end. This generates an electric field, or voltage, opposite to the carrier movement. The generated voltage can be described as

$$V = \alpha(T_1 - T_2)$$

where α is the differential Seebeck coefficient. The sign of α is positive if the generated voltage causes the current to flow in a clockwise direction and its magnitude depends on the choice of materials for the conductors. The coefficient is given in volt per kelvin [V/K]. The relation between the potential difference and the temperature difference can be seen as linear when dealing with small temperature differences [2].

8.2 Thermoelectric Element

A thermoelectric element consists of n- and p-type semiconductors. N-type semiconductors has a higher concentration of electrons, or negative charges. P-type semiconductors has a higher concentration of holes, or positive chargers. The semiconductors are electrically coupled in series, as shown in Figure 20, but thermally coupled in parallel. When heat is applied to one side of the thermoelectric element, top or bottom in Figure 20, the charge carriers diffuses and moves to the cold side causing a potential difference.

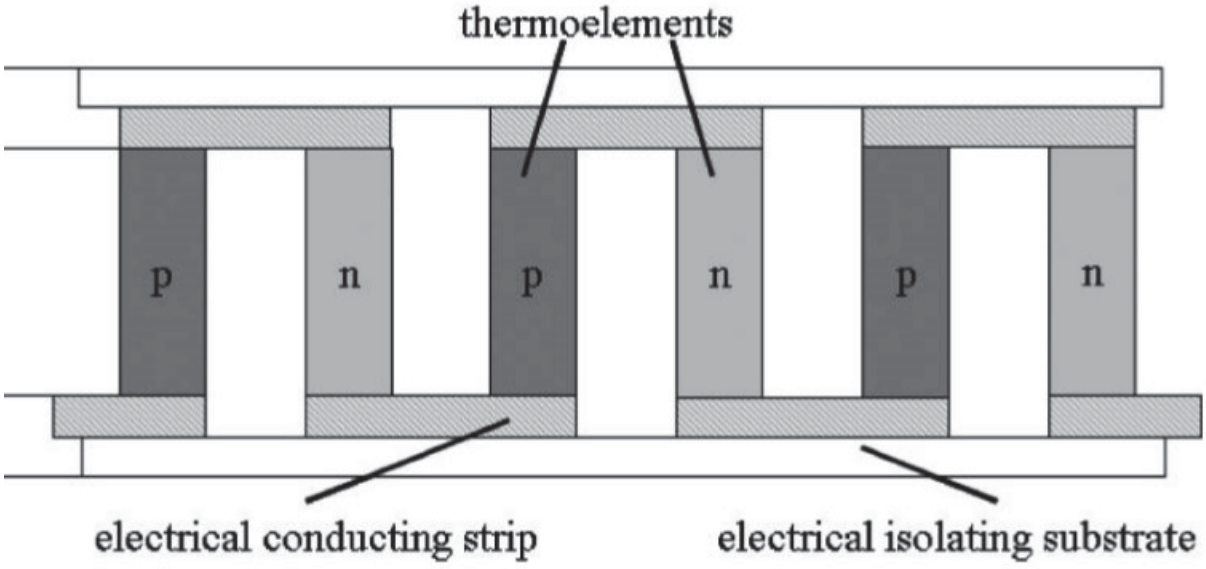

Figure 20. Principal configuration of a thermoelectric element, as demonstrated by Spies et al. [2].

Since the generated voltage from a TEG is dependent on a temperature gradient, it is important to maintain a temperature difference. This is done by through having a low thermal conductivity in the TEG and maintaining the temperature difference in the surrounding environment. This can make the TEG difficult to use as an EH transducer unless it is in a suitable environment and equipment like heat sinks are used.

There are not many commercial EH solutions utilizing TEGs on the market. One example is Micropelts Thin Film Thermogenerator MPG-D655, with an output power of about 6 mW at 30 K. The device is about 3,300x2,425x1,090 mm [28]. Another example of a promising concept application for TEGs is in combustion engines where they convert waste heat into electricity [29].

Table 8 shows some other available TEGs summarized by Spies et al. at a temperature difference of 100 K. It is common for TEGs that in order to get a usable amount of power, the temperature difference needs to be high. This makes the use of TEGs even more problematic. In Table 8, V_o is the open circuit voltage, I_s the short circuit current, R_i the internal resistance, G the thermal conductance of the module, G/A the thermal conductance per module area and $P1$ the power density.

Table 8. Summary of available TEGs.

Company	Type	$l \times w \times h$ (cm × cm × mm)	V_o (V)	I_s (A)	R_i (Ω)	α (V/K)	G (W/K)	G/A (mW cm^2/K)	P1* (mW/cm^2)	T_{max} (°C)
T	199-150-6	4 × 4 × 3.6	8.20	3.15	2.6	0.082	1.136	71	400	200
T	287-200-14	4 × 4 × 4.8	11.5	0.97	9.0	0.100	0.518	32	174	200
T	127-250-32	4 × 4 × 3.4	10.8	7.0	1.5	0.054	0.696	43	590	225
T	097-300-33	10 × 5 × 120	4.2	1.05	4	0.021	0.021		ca. 50	1000
M	240-100-50	0.5 × 0.7 × 0.5	1.20	0.15	8.0	0.024	1.388	4.1	110	150
N	N_x2	0.5 × 0.4 × 0.7	0.39	1.23	0.3			15	1500	
Hi-Z	HZ-2	2.9 × 2.9 × 5.1	3.2	0.8	4	0.032	0.4	47	148	250
Hi-Z	HZ-14	6.27 × 6.27 × 5	1.6				1.9	47	148	250

*At dT = 100 K; supplier: T, Thermalforce; M, Micropelt; N, Nextreme.

Examples of temperature gradients that can be exploited for EH with TEGs are: solar heat, ground soil to ambient air, water to ambient air, motor waste heat, aircraft compartments and industrial waste heat [2].

9 Power Control

EH transducers often have shifting polarities and a voltage output that is too varying or at the wrong level. Consequently, the power input has to be modulated to fit the load. This includes rectifying the current, converting the level of the DC voltage and matching the impedance of the load with the source.

9.1 Rectifiers

Since there are EH transducers that do not generate DC voltage, some require a rectifier to function. Furthermore, it is important that the rectifying is done as efficiently as possible since EH applications have a limited amount of power to use. Large voltage ripple has a negative effect on the output power of as well as the electronic components of the circuit. Using capacitors as filters after the rectifier will reduce the voltage ripple. The amplitude of the ripple will decrease with increased size of the capacitors although so will the responsiveness of the system [2]. Moreover, there has to be a storage element after the rectifier to make sure the energy can be used in the later stages of the EH system [30].

9.1.1 Graetz Bridge

A simple and common version for rectifying the current is the diode bridge or Graetz bridge. The diode bridge consists of four diodes that are biased as seen in Figure 21 to ensure the current travels through the load the right way no matter the polarity of the transducer voltage. The load in Figure 21 is defined as a voltage source connected in parallel with a current source and a resistor in series. The circuit is drawn in LTSpice XVII, as are all circuits in the Power control chapter.

Some of the transducers, such as piezoelectric elements, produce high voltages and are therefore relatively unaffected by the forward voltage drop of the diodes. Using a diode bridge for rectifying the current with these kinds of transducers might not present a problem. However, using a diode bridge with a high forward voltage could hinder or significantly reduce the effectiveness of lower voltage transducers such as dc-generators or magnetic transducers. Using diodes with as low forward voltage as possible gives the best efficiency. There is, however, often a trade-off between forward voltage and the maximum forward current meaning that systems with large amounts of input power need to use diodes with higher forward voltage. Schottky diodes are typically used for low forward voltage drops [31].

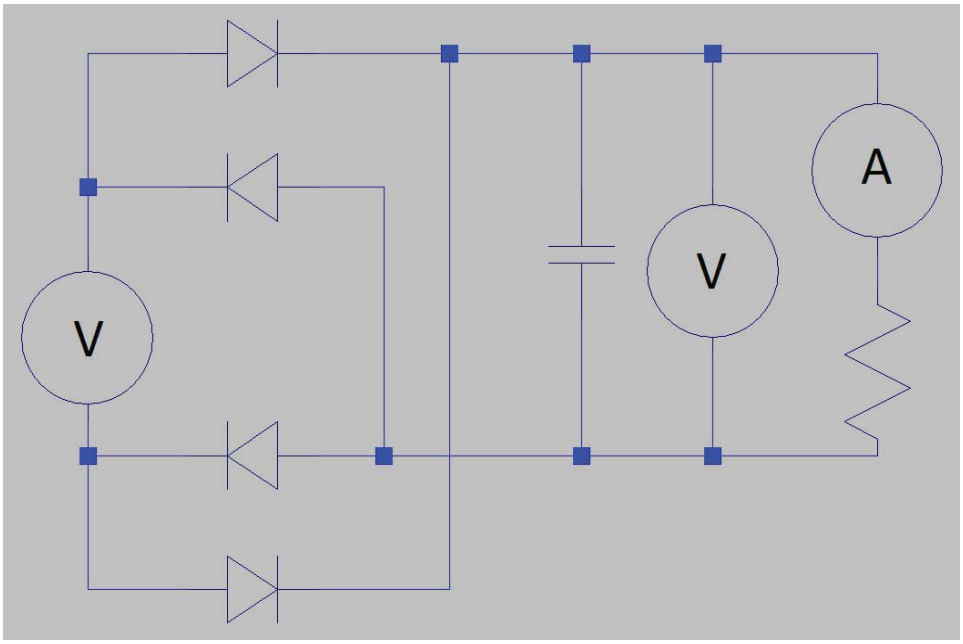

Figure 21. Graetz bridge rectifier connected to a voltage source and a load.

9.1.2 Voltage-doubler Rectifier

A voltage-doubler uses two capacitors, each connected to one side of the load as shown in Figure 22. The transducer is then, on one pole, connected between the capacitors and connected to a diode half-bridge on the other pole. The half-bridge is also connected to the load.

Assuming ideal components, no load and a sinusoidal voltage input, the amplitude of the voltage over the storage capacitor will be the same as the peak-to-peak voltage of the sine wave. For the first half of the sine wave coming from the transducer, the top capacitor will be charged. During the second half, the lower capacitor will be charged resulting in a potential difference twice the capacitor voltage over the load. Another capacitor added before the load will act as a buffer providing a more stable voltage.

Since the current only runs through one diode at a time, there is only one voltage drop affecting the output power from the transducer at a time. With the same diodes used, and capacitors with low enough parasitic properties, a voltage-doubler will therefore have a higher efficiency than a diode full-bridge rectifier [32].

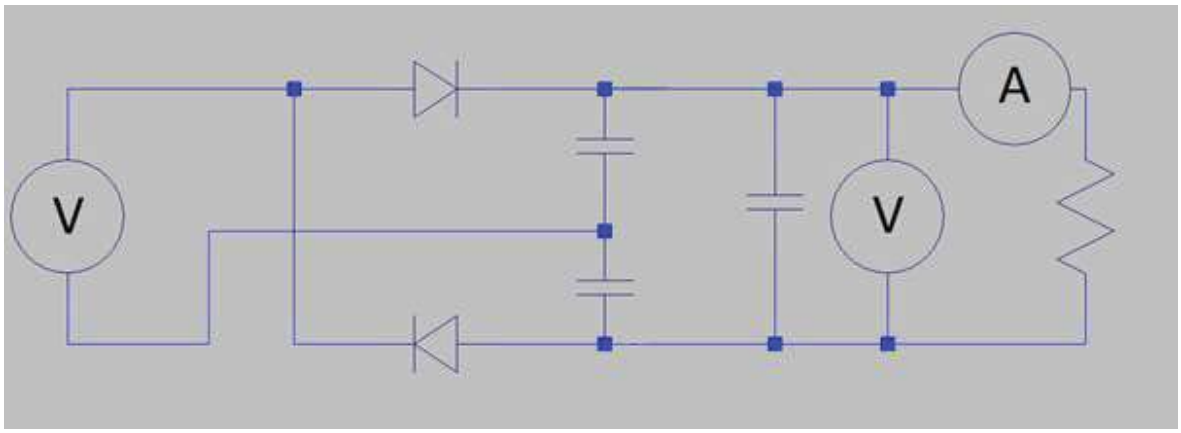

Figure 22. Voltage-doubler, as proposed in Optimization of rectifier circuits for a vibration EH system using a macro-fiber composite piezoelectric element [33], with an extra storage capacitor.

9.1.3 Greinacher Doubler Circuit

The Greinacher Doubler Circuit uses passive components to double the voltage form an alternating voltage source. The operation is similar to the voltage doubler since it is based on charging capacitors to ideally output a greater voltage than the input. The circuit first charges the upper capacitor, seen in Figure 23. Thereafter the lower capacitor is being charged to a level equal to the upper capacitors voltage and the voltage from the transducer combined.

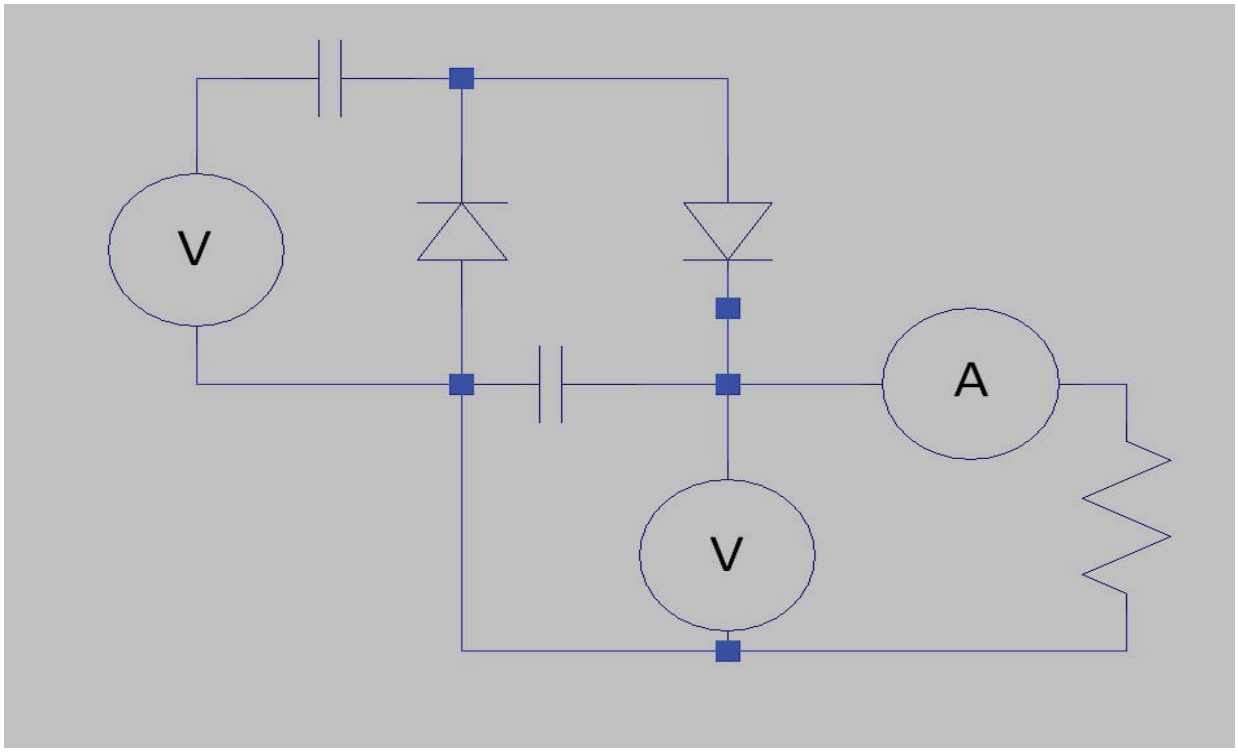

Figure 23. Greinacher Doubler Circuit.

9.1.4 MOSFET Bridge

The 4-switch H-bridge is built upon the same principle as the diode bridge except the diodes are replaced by MOSFETs. The gate of the MOSFETs is short-circuited to the drain, as seen in Figure 24, causing the potential between source and gate to become zero and the MOSFET operation to lie in the cut-off region. In the cut-off region, there will be no drain current and all of the current will go through the parasitic diode of the MOSFET [34]. The frequency response of this bridge is better than the diode bridge although the extractable power from the transducer is limited due to the limited current in the cut-off region [35].

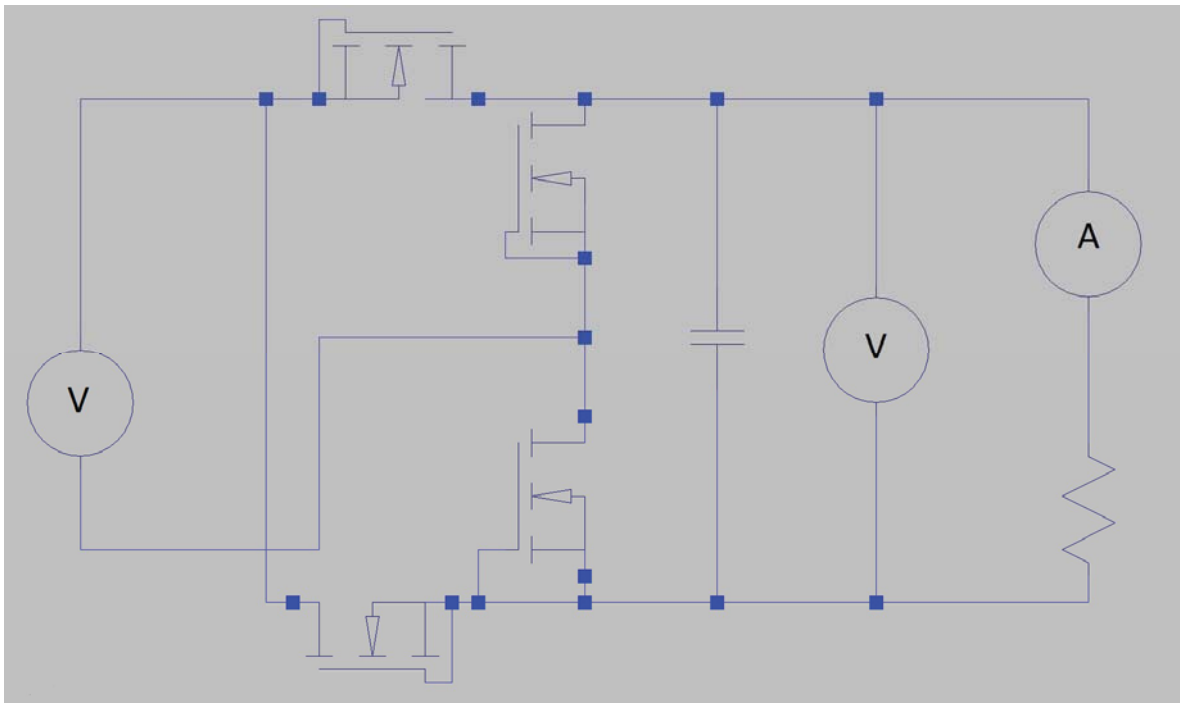

Figure 24. MOSFET bridge

9.1.5 Gate Cross-Coupled Rectifier

The gate cross coupled rectifier is a rectifier circuit used mostly in high frequency inductive coupling [31]. The rectifier is similar to the transistor bridge although it uses both pMOS and nMOS transistors. The gates of the transistors of one pole of the transducer are connected to the other pole, as seen in Figure 25, to achieve a gate-source potential equal to the potential difference between the poles of the transducer.

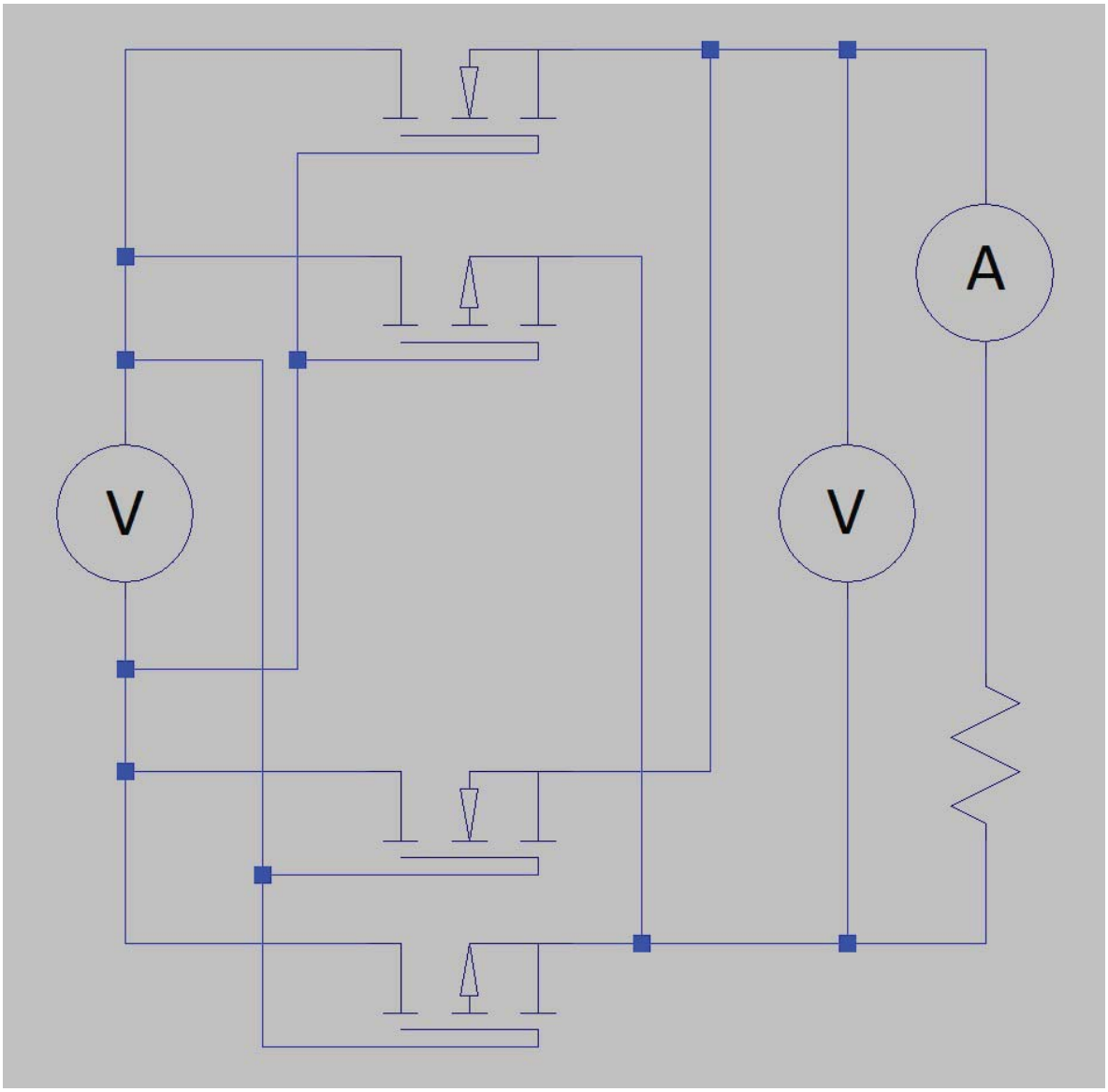

Figure 25. Gate Cross-coupled Rectifier

The rectifier is limited by the threshold voltage which the transducer must transcend to transfer power. This limits some low voltage EH transducers since the minimum start-up voltage increases. Ways of reducing the threshold have been developed as the threshold is a limiting factor for rectifiers. The threshold can be lowered by adding an external circuit supplying a voltage to the gate to cancel out the threshold voltage. This is called an external voltage cancellation [30].

A commonly used technique when working with complementary metal-oxide semiconductor is to use bootstrapping to reduce the threshold voltage of the transistors. To bootstrap the transistor, the input voltage is connected to the output through a capacitor. The capacitor is charged while the transistor is idle and discharged through parasitic resistance during operation [36].

The MOSFET transistors can also be exchanged for floating gate transistors. The floating gate (FG) transistors are programmed to have a high charge at the gate causing the transistor to carry current. Using FG transistors might lower the voltage drop over the transistor [37].

9.2 DC-DC Converters

To convert energy from transducers such as photovoltaic and thermoelectric transducers, which gives a varying and often low voltage, a DC-DC converter is needed. These are used to transform the voltage level and stabilize it. A problem in EH, due to the limited amount of energy available, is to produce converters with small losses. Another is to be able to convert very low voltage levels to usable ones. Especially RF harvesting has this problem since the voltage levels are usually in the microvolt to millivolt range [38].

9.2.1 Linear Regulators

The voltage conversion and regulation can be handled by a number of different types of regulators and converters. A linear regulator can be used to handle the conversion and the control of the voltage. The linear regulator is based on an operational amplifier, connected to the gate of a transistor, controlling the voltage to stay as close to a voltage reference as possible. This type of regulator is, however, not able to generate a bigger output- than input voltage [2]. This causes problems for several EH solution

s as they tend to have a low or uneven input voltage.

9.2.2 Switching Regulators

Instead of a linear regulator, a switching regulator can be used. As the name suggests, switching regulators converts the voltage through turning switches on and off. Switching regulators can be divided into four subtypes, buck converter, boost converter, flyback converter and forward converter.

Buck and Boost Converters

Buck converters deliver lower output than the input voltage and are therefore a better fit for high voltage EH transducers such as piezo elements. Boost converters offers a higher output than the input voltage and are therefore a better match for low voltage transducers such as TEGs. The buck and boost converters are built upon the principle of charging and discharging an inductor through a transistor.

The efficiency of a buck or boost converter depends on the equivalent series resistance of the inductor, the windings of the inductor, the resistance of the switches, the switching losses and the quiescent current of the controller. To optimize buck or boost converters efficiency, the size of the converter must be increased to host a larger inductor. A larger inductor can have a higher inductance with a lower equivalent series resistance than a smaller one [2].

Buck-boost Converter

For transducers spanning a larger voltage range, where the input voltage can be either above or below the application voltage, a buck-boost converter is able to produce either a larger or a smaller output voltage. The buck-boost converter is also able to produce a negative voltage compared to the input. It is built upon the same principle as the buck- and boost converters, with an inductor being charged and discharged through a transistor to control the voltage.

Flyback and Forward Converter

The flyback and forward converters utilizes transformers instead of an inductor to achieve a higher or lower voltage than the input. Flyback and forward converters offers isolation between the input and the output of the converter. However, this is not a necessary attribute in low power EH applications. The transformer will also need more space than the inductor of a buck-boost converter.

9.2.3 Dickson Charge Pump

A Dickson charge pump operates in a different way from the converters brought up so far in that it does not use an inductor to convert the voltage. The charge pump consist of a diode-bridge with capacitors connected to inverting switches as seen in Figure 26. This means that when the first inverter is low the voltage over the first capacitor, assuming an ideal diode, will be Vdd. The inverters are then switched meaning the potential over the second capacitor will be 2*Vdd. When the inverters are switched to high again, the potential after the second diode is 3*Vdd and so on. This way the voltage is “pumped”.

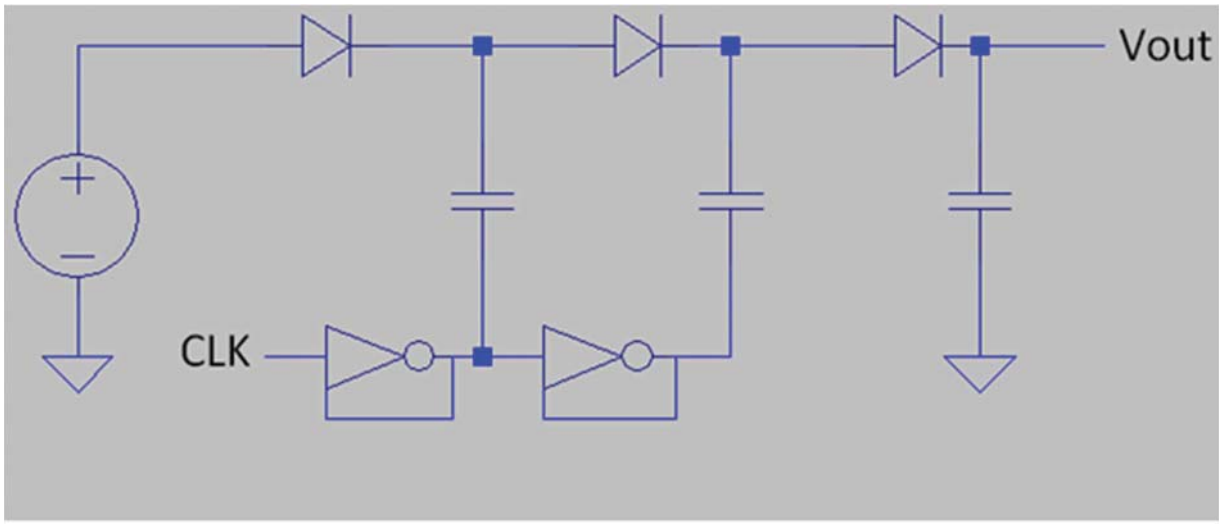

Figure 26. Dickson charge pump operated through two inverting switches.

The efficiency of the charge pump depends on the voltage drop of the diodes as well as the potential difference between the input and the output. Using switched transistors instead of diodes will increase the efficiency of the charge pump but will most likely be more costly and require more energy for low power EH applications. Charge pumps are often used to get usable voltages from RF EH as this often yields very low level of voltages.

9.2.4 Meissner Oscillator Based Converter

The Meissner oscillator based converter is a self-oscillating converter driven by a transformer. The converter uses an n-JFET with the gate connected to the transformer, as seen in Figure 27, to regulate the voltage. The default of the n-JFET is to conduct although when current is induced in the secondary winding of the transformer the JFET starts limiting the current. Having a self-oscillating converter could be more power efficient than controlling a circuit through drivers [2].

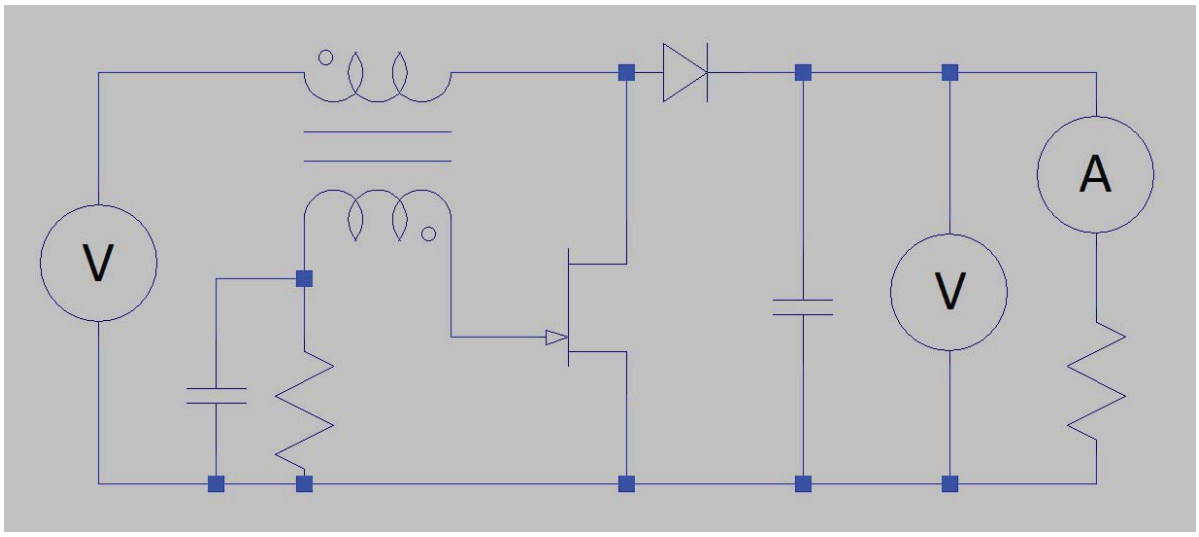

Figure 27. Meissner oscillator based converter.

9.3 Maximum Power Point Tracking

Some of the “ultra-low power” EH DC-DC converter ICs on the market today such as the LTC3105, LTC3588 and BQ25570 are aimed at high-impedance transducers such as piezo-elements or PVCs. This is due to the impedance matching that must be made to get a good efficiency.

EH transducers have properties causing the output current and voltage to depend on the load. There is a certain maximum output power to be found at a certain condition. This point is called the Maximum Power Point (MPP). If the characteristics of the load and the energy source are known, the EH circuit can be optimized. However, with a varying load or source, the MPP will also vary and therefore has to be tracked. To keep the voltage at the MPP, a method called impedance matching is used.

The load impedance can be fixed or adaptive. To make an adaptive load MPPT is used. Impedance matching is based upon matching the load impedance to the source impedance of the transducer. The load impedance is changed by changing the duty cycle of the converter. The source impedance can be calculated as the series resistance of a Thevenin equivalent of the transducer. According to Power Management Techniques for Integrated Circuit Design by Ke-Hong Chen [39], if the transducer is modelled as a voltage source with a source resistance and the load is purely resistive a matching efficiency of 90% will be achieved if the load impedance is 0.52 times the source impedance or if the load impedance is 1.93 times the source impedance as seen in Figure 28.

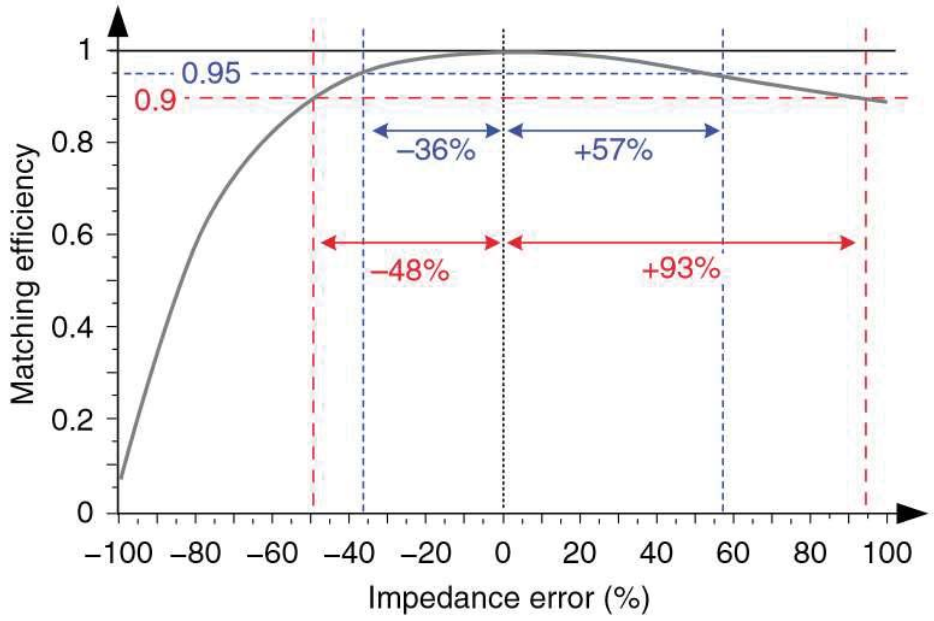

Figure 28. Matching efficiency versus impedance error of an EH transducer modelled as a voltage source and a source resistance and a resistive load.

9.3.1 Mountain Climbing Method

There are various ways of finding the MPP. A commonly used one is the mountain climbing method. The mounting climbing method works through starting at a very low load impedance and then increasing the impedance of the load in small steps until the output power no longer increases. When the power decreases instead of increases, the tracker starts searching for the MPP in the other direction. This means that when the MPP has changed the MPPT will start climbing towards it. It is possible for an EH transducer to have local MPPs. In this case the mounting climbing method could get stuck on a local maximum [39].

When designing a mounting climbing MPPT, the step size is important. A small step size will require more processing power, faster sampling and getting stuck at local power points, resulting in higher power losses. A larger step size risks oscillating around the MPP.

Using this method means that there has to be a constant sampling and comparison of the power. Therefore it is also consuming relatively high power levels for low power EH. Using a microcontroller or something similar to do the readings and control would also require another power source. This reduces the usefulness of low power EH.

9.3.2 Incremental Conductance-method

The incremental conductance-method controls the duty cycle based on the power derivate with respect to voltage. When the power derivate is zero, a local maximum has been found:

$$\frac{dP}{dU} = 0$$

When derived from the power equation, the power derivate can be written as:

$$\frac{dP}{dU} = \frac{d(U \cdot I)}{dU} = I + U\frac{dI}{dU}$$

Combined with the criteria for the local maximum:

$$-\frac{I}{U} = \frac{dI}{dU}$$

If the transducer voltage is lower than the maximum power point voltage, the incremental conductance is greater than the negative conductance. If the transducer voltage is higher than the maximum power voltage, the incremental conductance is lesser than the negative conductance.

The MPPT will need to adjust the impedance until the MPP is found. It will continue to check dI until the equation no longer holds. An increase in current means the voltage should be incremented and a decrease in current means the voltage should be decremented.

The incremental conductance-method is more useful than the mountain climbing method for conditions where the MPP changes quickly since the direction of the MPP is known [39]. Since this method is relatively calculation heavy, it requires a microcontroller. Therefore, for low power EH applications, a very low power microcontroller is required and the ability to provide it with a sufficient voltage.

9.3.3 Open-circuit Test Method

If the transducer has a fixed impedance, the MPP will depend on the input energy. In this case the open-circuit test method is used. The open-circuit test method measures the open circuit voltage and compares it to the load MPPT voltage. To measure the open-circuit voltage, the load has to be disconnected from the transducer. However, the comparison can be done while the circuit is closed.

Some transducers such as TEGs and PVCs have ratios between the open-circuit voltage and the MPPT voltage that do not differ much with external conditions. This means that control with fixed ratios can be used with good efficiency. Since the open-circuit test method only has to charge a couple of capacitors and compare, it is also faster than the mounting climbing method.

Instead of comparing the open-circuit voltage, the ratio between the MPP current and the short circuit current can be used. In this case the transducer has to be short circuited during a short interval while the current is being sampled. The rest of the circuit could be powered with a buffer capacitor during the sampling period [8].

9.3.4 Constant Voltage Method

If the MPP is believed to be static during operation, a constant voltage reference can be used to control the voltage. In practice, the achieved voltage won't be at the MPP although in some cases it will be close. The MPP is typically made through running a constant current through a resistor. The MPP can then be adjusted by altering the resistance. If a thermistor is coupled to, for example a PVC used as a transducer, the reference voltage can be adjusted based on the temperature. Since the temperature based behavior of a PVC is often known from datasheets, this can be used as a reliable MPPT.

When using an MPPT system, the power consumption of the MPPT versus the power saved from losses

has to be considered. Since many EH applications have very low input power, the MPPT could consume a significant amount of the available power. If the MPPT consumes a higher amount of power than what is gained through finding the MPP, the MPPT system is redundant. Some MPPT systems also require some logic or control to be carried out and need a microcontroller or FPGA to do this. These components need either the input voltage to be high enough or a power supply of their own to be able to function. This will add cost and reduce the viability of the system and therefore also has to be considered when making total cost calculations of the system.

Using an MPPT will cause the transducer to operate at its maximum energy level. However, if the converter needs a certain voltage to operate, the MPPT will bring the output voltage below usable levels in certain conditions. The properties of the transducers and the environment must be known to ensure that the MPP does not fall below acceptable voltage or current levels.

10 Energy Storage

Storing energy in between blocks of an EH system is vital since the amount of energy being harvested often varies over time. Without storage buffers excess energy is lost. The energy storage has to be tailored to the transducers energy cycles and the applications duty cycle to be able to supply the application with sufficient power at all times. In EH applications the most used storage components are lithium-ion batteries, capacitors and supercapacitors. The different storage components have different attributes and are appropriate to use for different applications.

Batteries are divided into different categories based on their function. A primary battery is a battery with an irreversible chemical process. Secondary batteries have a reversible chemical process. They are able to be charged and discharged multiple times [40]. When comparing batteries, the properties of the batteries are discussed in terms of energy density and power density. Energy density specifies how much energy a battery can store per volume [J/m^3]. Power density states how much power a battery can deliver per volume [W/m^3] [40]. Rechargeable batteries have energy densities up to 600 Wh/l while non-rechargeable ones have an energy density of up to 1400Wh/l.

In the case of EH systems for low power applications, batteries with relatively low total energy are used to get a better charge rate. This means that the batteries often have a small volume. When comparing small batteries, the casing of the battery corresponds to a large part of the battery's total volume. The power- and energy density units are therefore only good metrics when comparing batteries of the same size as the energy density decreases rapidly with size [2].

10.1 Lithium-ion Batteries

Lithium-ion, or Li-ion, batteries lose capacity over time. The degradation of the batteries depends on the temperature, the number of charge cycles and what voltage the battery is kept at. All temperatures deviating from the recommended temperature have a negative effect on the battery life. Furthermore, the capacity is usually reduced with each charge cycle a battery is exposed to. Keeping the battery close to the maximum charge for long periods of time also has a negative impact on the battery life. This can be mitigated by reducing the maximum charge level by a small amount. At this point in time, hermetically sealed Li-ion batteries have a life span of up to 20 years. However, a battery in use has a considerably lower life span [2].

Improvement in Li-ion energy density is continuously being made. However, the increase rate typically lies around a few percent per year [41]. Part of the research focus with Li-ion batteries is to increase the stability of the batteries to allow longer life spans. On the other hand, the required energy of battery driven electronic systems are expected to decrease by a factor of 10 to 100 over the next decade [2]. In theory, this would allow batteries to power these systems for 30 years or longer if battery degradation could be stopped.

However, batteries have some downsides since they are susceptible to the surrounding environment to a larger degree than the rest of the EH system [2]. Li-ion batteries also contain some chemical elements that are getting rarer, such as cobalt and lithium. The manufacturing emissions from Li-ion batteries tend to be high as well [42]. However, research is being done into replacing lithium with other metals such as sodium [41]. Furthermore, Li-ion batteries can be overcharged when used in an EH system with risk of

damage to both the application and its surroundings. Therefore some sort of battery protection should be added.

The properties of Li-ion batteries change based on the materials the cathode and anode are made of. Lithium cobalt oxide is the most commonly used alloy for the cathode. However, there are other alloys used in commercial batteries such as lithium manganese oxide, lithium nickel oxide, lithium nickel cobalt manganese oxide and lithium iron phosphate. Lithium manganese oxide has a lower than average energy density but provides a higher cell voltage. It is also friendlier towards the environment and can withstand higher temperatures. Lithium nickel oxide has the highest energy density with a low cell voltage. Lithium iron phosphate is the most thermally stable alloy and will not combust from overcharging [2].

The anode of most Li-ion cells is made out of a lithium carbon alloy. Lithium titanate alloys are used as well since they provide a higher power density at the expense of a lower cell voltage and energy density.

Li-ion batteries normally have fluid electrolytes although they can also be made in a solid-state thin-film variant. These are limited to a thickness of a few micrometers and have high production costs. Coin-type batteries are currently the cheapest Li-ion batteries to make while thin-film batteries are the most expensive. Thin-film batteries are however easy to minimize and there is no risk of electrolyte leakage [2].

Several different new manufacturing processes of Li-ion batteries are being researched. Two problems with solid-state thin-film batteries are the limited geometry and the high manufacturing costs. These batteries are otherwise better suited as secondary batteries for EH as they have long life spans and high power density. With improvement in the manufacturing of these batteries, advances in the energy storage of EH could be made with longer life spans and lower self-discharge rates [2]. A new breakthrough in solid-state Li-ion battery technology was recently made where the electrolyte of the battery was exchanged for an Na-ion glass electrolyte. This could reduce manufacturing costs while increasing energy density and lifecycle [43].

10.2 Supercapacitors

Another alternative to using Li-ion batteries in EH products is to use supercapacitors. The chemical structure of the supercapacitor causes them to have a lower energy density than batteries. The charge and discharge rates of the supercapacitors are faster, providing a higher power density. Supercapacitors have a less limited amount of charge and discharge cycles. However, the self-discharge rate of supercapacitors is greater than batteries [2]. Supercapacitors can be divided into three different capacitor types, electric double-layer capacitors (EDLC), pseudocapacitors and hybrid capacitors . EDLC are the most commonly produced ones for commercial use and have some advantages over the other supercapacitor-types such as being able to operate in a large temperature interval [44].

Supercapacitors have other advantages over batteries specific for EH applications. The way EH systems are designed tend to require a high charge and discharge rate resulting in a high number of charge and discharge cycles. Furthermore supercapacitors have a higher charging efficiency than batteries [40]. The charging efficiency of Li-ion batteries does not exceed 70% [41] whereas supercapacitors have a negligible loss while charging [45]. Since the function of EH systems are power dependent, having an efficient system is of importance. EH systems are sometimes placed outdoors where ambient

temperatures might be outside of the ideal operating range for batteries. Supercapacitors have a broader working temperature range allowing them to be used in applications where temperature might be an issue.

The maximum energy stored in an ideal supercapacitor can be calculated as [41]:

$$E = \frac{1}{2}C \cdot (U_{max}^2 - U_{min}^2)$$

Which can be used to calculate what size a capacitor would need to be to power a load within a certain voltage span in a certain time interval. Since EH applications need a power supply during a set time to gather data, send signals etc. the size of the capacitor has to be matched to the load.

10.3 Energy Budget Calculation

A distinction between different kinds of load in EH can be made. There are continuous and discontinuous loads. Continuous loads are always powered up and have cycles where there is a significant difference in power consumption depending on the task. An example would be a WSN-node sending data every few seconds to go into a sleep mode when not sending anything. The other load, a discontinuous load, is a load that is drawing power until it is unable to operate. Data being sent each time a button is pushed would be an example of this. These loads are useful in combination with transducers irregularly providing energy to the system.

To make sure an EH system is able to power a load during a specific interval of time, an energy budget has to be set up. Assuming a continuous load, the energy budget can be set up for two different subcases. The first case bases the calculation on the maximum power consumption of the load. The budget can also be set up for a set duty cycle for the load, where the average power in has to be greater than the average load. It could also be based on a discontinuous load where the load only has power when there has been an inflow of energy. In this case the energy provided during a certain time interval has to be greater or equal to what the application requires to complete a task.

When calculating if a load can be continuously powered by a transducer, the available power in the storage must be greater than the maximum power consumption of the load. If the transducer is able to continuously supply more power than what is required to operate the application at any given time, there is no need for energy storage. However, the storage adds filtering and makes the application more reliable since finding an ideal energy source for the transducer is impossible in practice. What is more, whenever the available power is lower than what the load requires, all energy is lost. Also, all excess power is lost when the available power is greater than what the load requires. Given a large enough storage component, the average load during operation can be used for calculation instead [46].

To calculate the energy budget, a model of the load and the source should be set up. The power supply to the system could be seen as a varying power input, P_{in}, in a finite time, T. If the energy supplied to the system over the time T is then assumed to be constrained by two outer limits $E_{varying,in,1}$ and $E_{varying,in,2}$, the energy going into the system could be expressed as

$$P_{const,in}T + E_{varying,in,2} \geq \int_T P_{in}(t)dt \geq P_{const,in}T - E_{varying,in,1}$$

The load can then be constrained as

$$\int_T P_{load}(t)dt \leq P_{const,load}T + E_{varying,load}$$

The system will be able to supply the load indefinitely if there is a storage capacity of $E_{varying,load} + E_{varying,in,1} + E_{varying,in,2}$ and $P_{const,in} \geq P_{const,load}$ [46]. However, this assumes an ideal energy storage component. If the energy storage component is not ideal but a Li-ion battery or a supercapacitor instead, the energy budget has to consider the leakage, charging efficiency and capacity loss over time [47].

11 Low Power Microcontrollers

The amount of energy harvested from micro EH is usually low. From this follows that the applications are limited to a low power consumption. Central to almost all EH applications is a Microcontroller Unit (MCU). This section will go through the key factors to lowering the power consumption of an MCU.

An MCU consists of at least one Central Processing Unit (CPU), a memory and programmable Input/Output (I/O) peripherals. It usually has multiple energy modes. Each mode allows a certain set of capabilities which requires a certain amount of current. A higher set of capabilities requires a higher amount of current. A lower set of capabilities requires a lower amount of current, but the functionality of the CPU, memory and I/O peripherals are lowered. An MCUs capabilities can to some extent be defined by the peripherals it controls. These can be grouped into the following four categories [48]:

- High frequency peripherals
    - Clock frequency in the MHz range
    - Example: UART, USB, high frequency timers, Direct Memory Access (DMA), etc.
- Low frequency peripherals
    - Clock frequency usually in the 32 kHz range
- Asynchronous peripherals
    - No clocks used
    - Respond to externally generated events like a pulse counter or an interrupt
- IO state and wakeup
    - Ability to wake up and give control back to software
    - Ability to retain state of the MCU pins

Low power modes usually range from light sleep or standby mode to deep sleep and off. The specific functionality of each mode varies between MCUs, but the idea is the same. That idea is: the deeper the sleep, the less power is consumed.

11.1 Sleep

In sleep mode, the clock that drives the CPU is disabled. However, the high frequency clock oscillator remains running which means that the CPU is able to resume executing instructions if it is woken up.

In standby mode, the clocks that drive the high-frequency peripherals are usually kept active. This allows functions like DMA, high-speed serial ports, A/D converters and D/A converters to function autonomously. Random Access Memory (RAM) remains active and can be accessed by the DMA. The DMA and RAM allows data from the peripherals to be stored without CPU intervention.

The advantage of sleep or standby mode is the simplicity. The MCU can with the help of an interrupt simply return to active mode with little delay due to preservation of the MCUs pointer and configuration registers. However, the advantage of simplicity and the high level of responsiveness comes at the cost of a relatively high current consumption.

The current consumption of sleep or standby mode can range from 45µA/MHz for an energy-optimized MCU to more than 200µA/MHz [49].

11.2 Deep Sleep

The MCU can enter an even lower energy mode by disabling high-frequency clocks and other non-essential loads. The high frequency MCU oscillator is disabled but the oscillator used to drive critical peripherals is kept running, for example the real-time clock. This is called deep sleep. Exactly which peripherals are kept enabled or not is application specific. Sometimes it might be more efficient to keep serial ports, touchscreen interfaces, or LCD drivers active to allow the system to process I/O without waking the CPU until it is absolutely necessary. That way it can save energy in deep sleep mode for a longer time. In other applications the designer may choose to have the pulse width modulation active to control a motor or detect external pulses. According to the datasheets from various manufacturers of MCUs (Texas Instruments, Atmel, Microchip, Silicon Labs), MCUs in deep sleep mode, Energy Mode 3 (EM3) in Figure 29, have a current consumption of about 0.1-10 µA and a wake up time of about 1-100 µs.

To save even more energy, the MCU can be stripped of all but minimum functionality to trigger a wake-up from an interrupt during deep sleep. In this mode all functions and clocks are powered down except for interrupt monitoring and the wake-up function. To restart the MCU you need to reset it or send an interrupt signal. The energy savings from doing this comes at the cost of a significantly longer wake-up time. When the MCU starts to wake up, it needs to power up its high frequency clock generator and stabilize before the CPU can load memory contents from backup storage and execute its first instruction. In this mode, the power consumption can become as low as 20 nA, but the wakeup time can increase to 200 µs [49].

A generic overview of the different states of an MCU and the transitions between them is given in Figure 29.

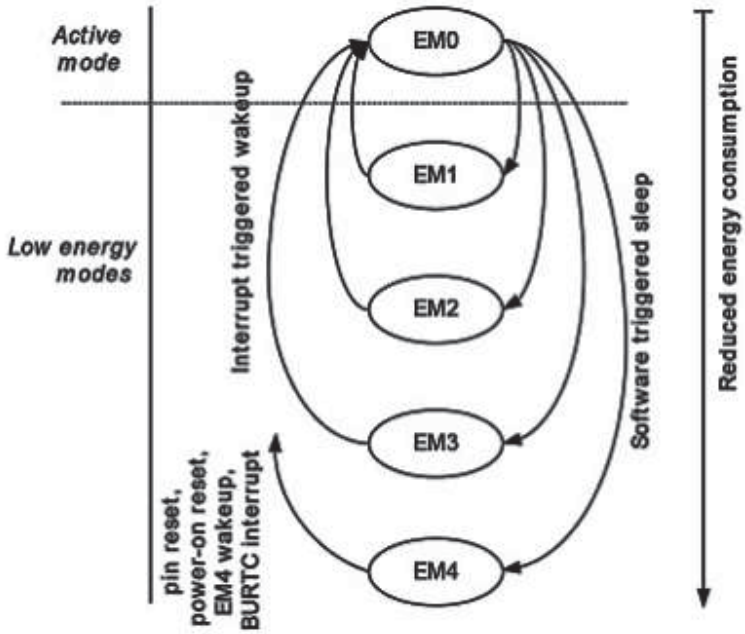

Figure 29. A generic overview of the different states of an MCU and the transitions between them [49].

11.3 CPU Clock Speed

In conclusion, a key factor to lowering the power consumption of the MCU is to disable the CPU as much as possible. However, it will eventually have to perform some work and therefore the choice of processor is essential for the power consumption of the MCU. A common rule is to use a CPU with as low clock speed as possible, but this is not always the case. The faster the CPU works, the more time it can spend in sleep mode. This is illustrated in Figure 30. In the upper diagram, a CPU with a low clock speed is used and in the lower diagram a CPU with a faster clock speed is used. The green area represents the current consumption of the CPU. The grey area represents a third CPU with a high current consumption, with the purpose to illustrate the reduced current consumption.

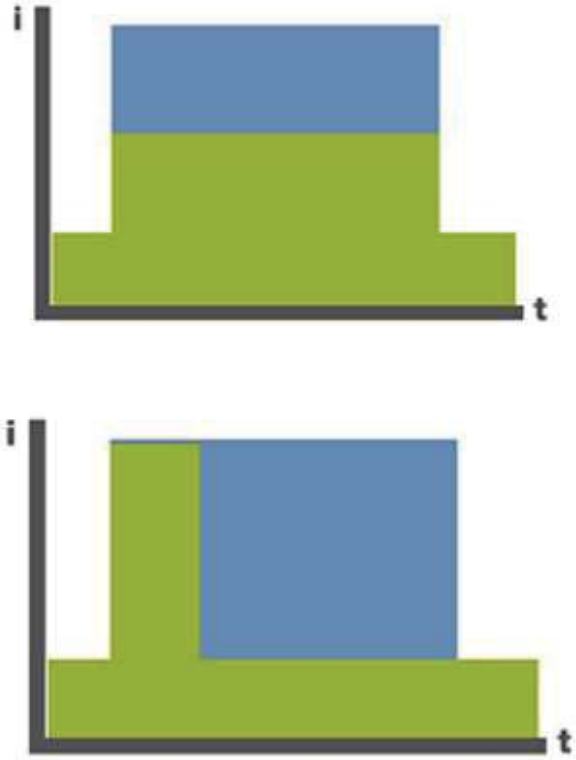

Figure 30. Diagrams describing the current consumption of two different CPUs with different clock speeds. The green area represents the current consumption of the CPU. The grey area represents a third CPU with a high current consumption [49].

11.4 Summary

There are many mechanisms to consider when designing low power MCUs and both hardware and software needs to be optimized. The most important factors to take into consideration when choosing a low power MCU are summarized below [50] [51] [49]. The designer will have to prioritize between them depending on the application.

- Optimized CPU clockspeed
- Low active power consumption
- Reduced Processing Time
- Fast Wake-up Time
- Low standby current
- Operate the peripherals without involving the CPU as much as possible
- Power efficient peripherals
- Optimized energy modes

12 Tests

12.1 Testing of Photovoltaic Cells

Two different PVCs are tested. The first one is a monocrystalline PVC from IXYS, KXOB22-12X1L, intended for outdoor use. The second is an amorphous PVC from Panasonic, AM-1417, intended for indoor use. The data from the datasheet of KXOB22-12X1L [11] is shown in Table 9 and the data from the datasheet of AM-1417 [52] is shown in Table 10. IXYS do not provide a value for the output power in an indoor environment. They state that the value of the maximum output power at 1 sun shall be divided by 200 to 500 to get an idea of how the PVC will perform in indoor environments with fluorescent lightning. Panasonic only provides an output power at 200 lux.

Table 9. Data from the datasheet of IXYS KXOB22-12X1L.

Manufacturer	**Model**	**Type**	**Open circuit voltage, Voc (V)**	**Short circuit current density, Jsc (mA/cm²)**	**Voltage at max. power point, (V)**
IXYS	KXOB22-12X1L	Mono-crystalline	0.630	42.4	0.501
Current density at max. power point (mA/cm²)	**Power at max. power point @ 1 sun (µW)**	**Area (cm²)**	**Divided by 200 (µW)**	**Divided by 500 (µW)**	**Power Density Divided by 500 (µW/cm²)**
37.2	18600	1.54	93.0	37.2	24.2

Table 10. Data from the datasheet of Panasonic AM-1417.

Manufacturer	**Model**	**Type**	**Open circuit voltage, Voc (V)**	**Short circuit current, Isc (mA)**	**Short circuit current density, Jsc (mA/cm²)**
Panasonic	AM-1417	Amorphous	2.4	0.0135	0.00277
Typical voltage @ FL - 200 lux (V)	**Typical current @ FL-200 lux (mA)**	**Typical power @ FL-200 lux (µW)**	**Area (cm²)**	**Typical power density @ FL-200 lux (µW/cm²)**	-
1.5	0.125	18.75	4.865	3.85	-

12.2 Power Management Boards

Two different power management boards are used to test the PVCs. The first one is based on the integrated circuit (IC) LTC3105 [53] from Linear Technology and the second one is based on the IC BQ25570 [7] from Texas Instruments.

12.2.1 LTC3105

The LTC3105 is a Step-Up DC-DC Converter with an MPPC. It has a cold start-up voltage of 250 mV and a programmable output of 1.6 to 5.25 V. Burst mode operation is used to output voltage.

To use the LTC3105, a PCB is designed in Autodesk Eagle and ordered from a PCB manufacturer. Pads for connecting a battery and a shunt battery charger system with a low battery disconnect, LTC4071 [54], are included but not used in the testing. The electronic design is shown in Figure 31 and the PCB schematic is shown in Figure 32.

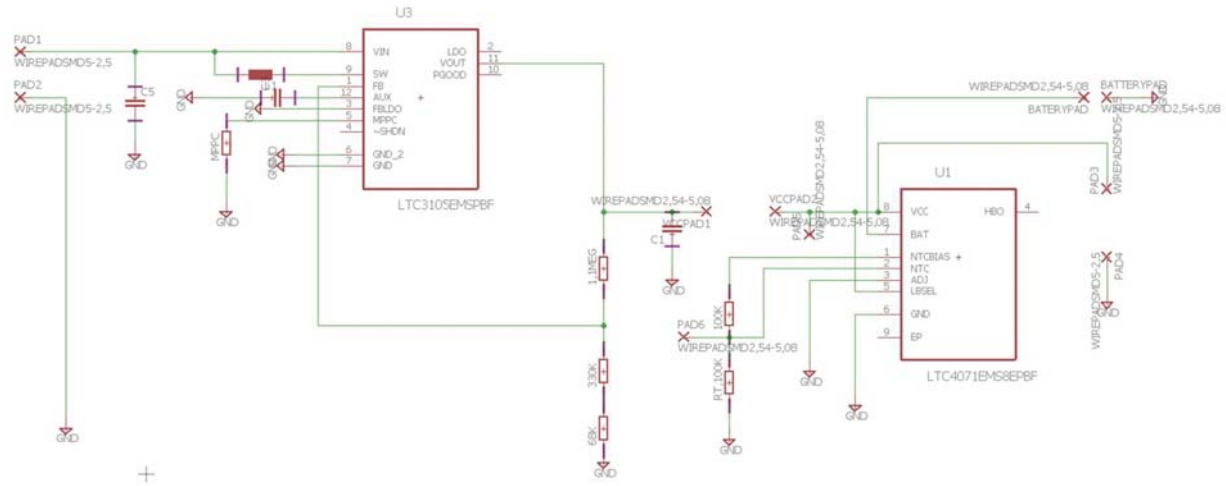

Figure 31. Electronic design of the LTC3105 testing board.

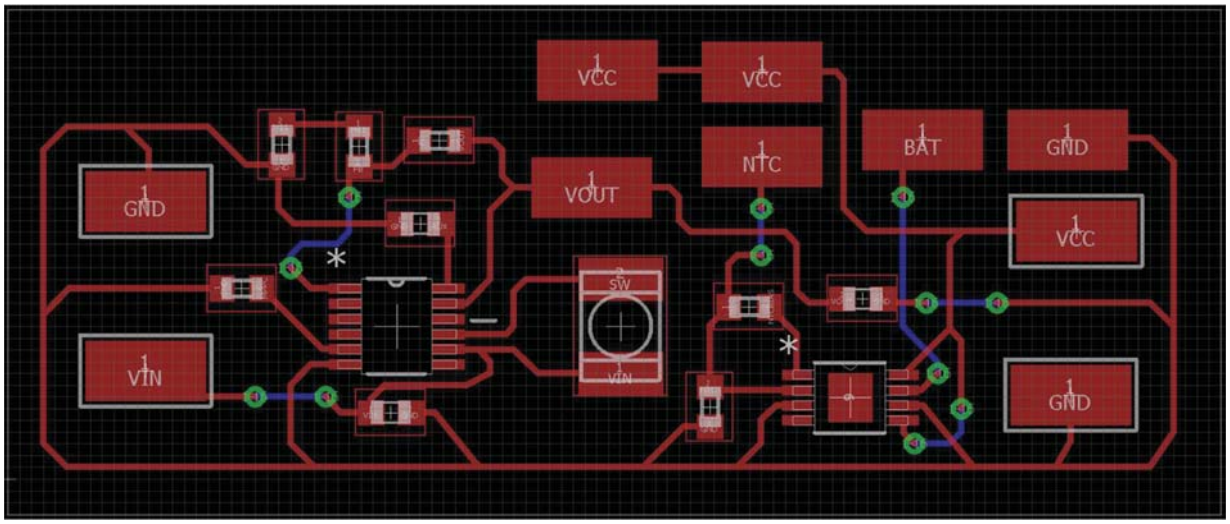

Figure 32. PCB schematic of the LTC3105 testing board.

The photovoltaic cells are connected to PAD1 and PAD2 Figure 31 in or VIN and GND in Figure 32. A battery can be connected to the BATTERYPADS and a load can be connected to PAD3 and PAD4 (VCC and GND) in Figure 31. LTC4071 is connected to VOUT from LTC3105 via VCCPAD1 and VCCPAD2. The reason for using the pads is simply to be able to disconnect the LTC4071 if it is not needed. PAD5 and PAD6 are used to be able to configure the properties of the LTC4071 by connecting NTC to VCC according to the datasheet [54]. The output voltage from LTC3105 is programmed by choosing the resistance, R_1, between VOUT and FB and the resistance between FB and GND, R_2, according to

$$V_{out} = 1.004 * \left(\frac{R_1}{R_2} + 1\right)$$

R_2 is in this case divided into two resistors to provide the possibility to combine different resistors to get the desired value. The MPPC of LTC3105 uses the Constant Voltage Method and is programmed by choosing the MPPC resistor according to

$$V_{MPPC} = 10^{-5} * R_{MPPC}$$

10^{-5} is the magnitude of the current flowing through R_{MPPC}. A 4.7 µF capacitor is inserted between LDO and GND. The other capacitors, inductors and resistors are chosen based on the information provided in the datasheets.

12.2.2 BQ25570

To use the BQ25570, the BQ25570 Evaluation Module (EVM) [55] from Texas Instruments is used. BQ25570 with pin names is shown in Figure 33 and the BQ25570 EVM is shown in Figure 34. The BQ25570 contains a boost converter and a programmable step down regulated output. It also contains an MPPC and a battery charge protection. It requires an input voltage, VIN_DC, of 330 mV to cold-start but can function from input voltages being as low as 100 mV after that. The boost charger output pin is VSTOR. Once VSTOR is above VSTOR_CHGEN, typically 1.8V, the boost charger can effectively charge a battery connected to the VBAT pin. A battery over- and under voltage protection can be set, VBAT_OV and VBAT_UV. A load can be connected to the buck converter through the VOUT pin. The buck converter is disabled when the voltage on VSTOR drops below the VBAT_UV limit. BQ25570 has a recommended VOUT and VBAT of 2-5.5 V. The MPPC uses the Open Circuit Test Method and can be programmed to 80 % of the V_{oc} for PVCs by tying VOC_SAMP to VSTOR, or 50% of the V_{oc} for TEGs by tying VOC_SAMP to GND. The MPPC can also be set by using external resistors according to:

$$VREF\_SAMP = VIN\_DC(OpenCircuit)\left(\frac{R_{OC1}}{R_{OC1} + R_{OC2}}\right)$$

R_{OC1} is located between VRDIV and VOC_SAMP and R_{OC2} between VOC_SAMP and GND.

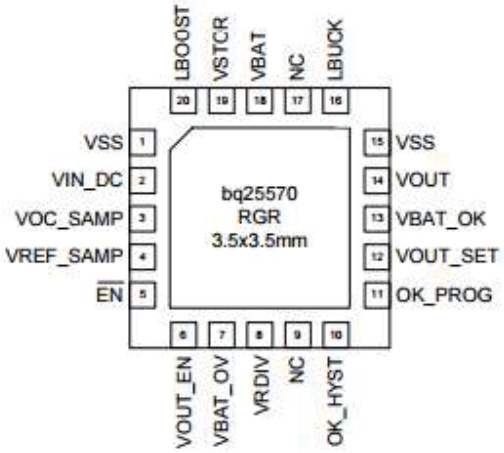

Figure 33. BQ25570 with pin names [7].

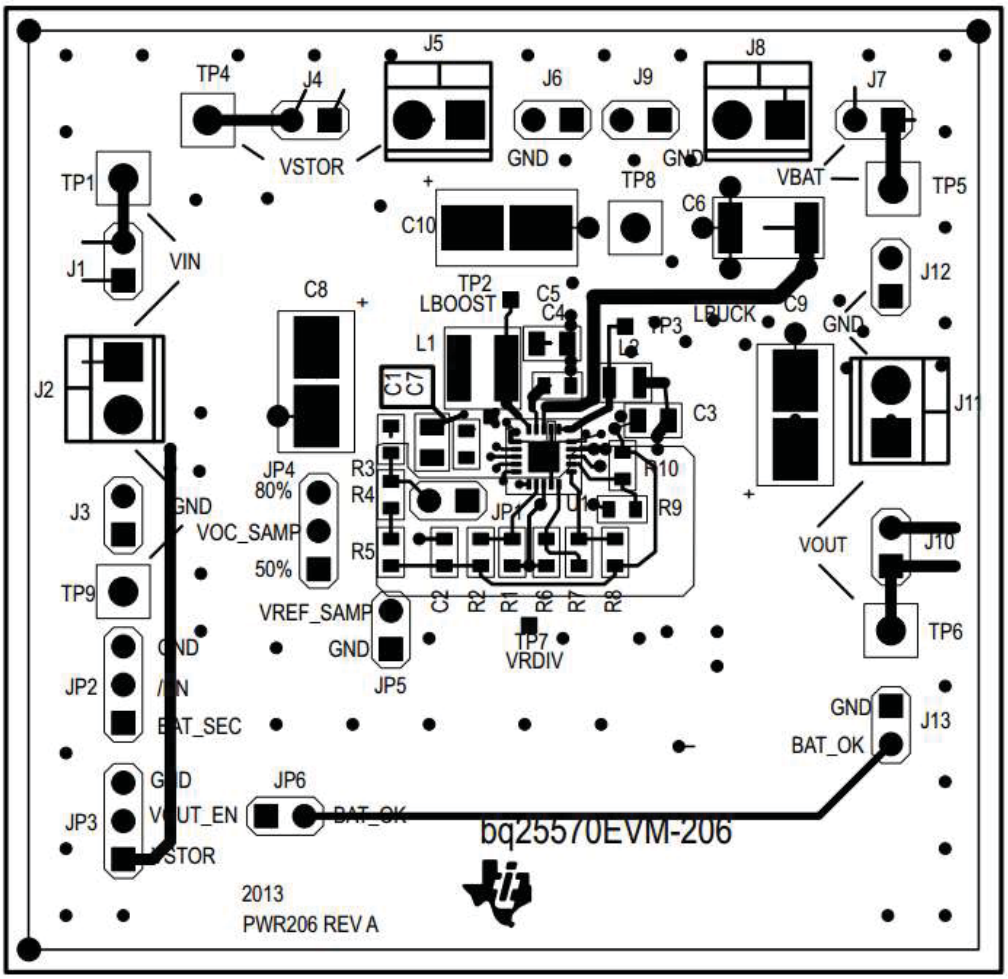

Figure 34. BQ25570 EVM [55].

12.3 Test Set-up

The PVCs are tested in two different environments, indoor fluorescent office light and outdoor bright sunlight. The indoor tests are done at 302 – 346 lux and the outdoor tests are done at 41000 – 47800 lux measured with a SEKONIC Flash Master L-358 [56].

The PVCs power output in different configurations is tested to find the best power densities. The testing is done by charging a supercapacitor of 0.1 F. The supercapacitor is rated at 5.5 V. The charging behavior of the best PVC type and configuration is also investigated.

LTC3105 is configured to output 3.53 V. The LTC4071 charge protection is never used, since LTC4071's low battery disconnect level of 2.7 – 3.2 V and a float voltage of 4.0, 4.1 or 4.2 V does not match small rechargeable batteries like 1.5 V or 3.3 V.

When using BQ25570 EVM, the PVCs are connected to VIN and GND. The supercapacitor is connected to VBAT and GND. VBAT is programmed to 4.2 V.

The two equations used when the output power is calculated are shown below. E is the energy stored in the supercapacitor, C is the capacitance, U is the voltage over the capacitor and dE is the difference in energy during the time interval dT. The voltage U is measured with a voltmeter and the time interval dT is measured with a stopwatch.

$$E = \frac{1}{2} * C * U^2$$

$$P = \frac{dE}{dT}$$

The configuration of the PVCs in the test results is denoted as row x col. Row is the number of PVCs in series and col is the number of these series that are parallel coupled. An example is shown in Figure 35, where AM-1417 is shown in a 4x1 configuration and KXOB22-12X1L shown in a 3x4 configuration.

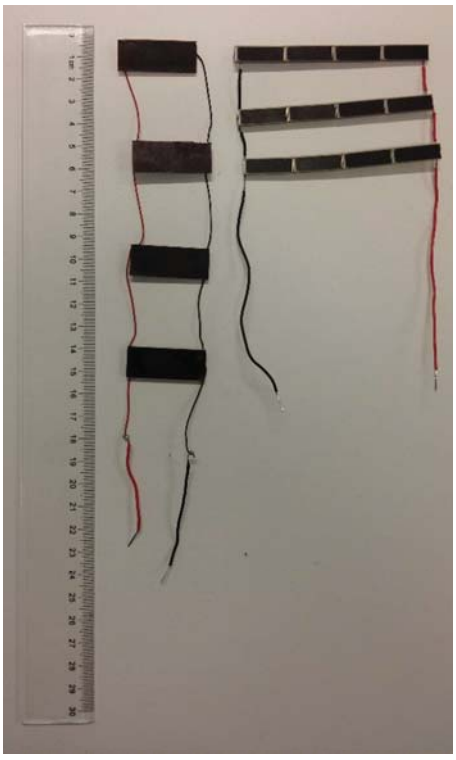

Figure 35. To the left, AM-1417 in a 4x1 configuration. To the right, KXOB22-12X1L in a 3x4 configuration.

12.4 Testing of DC-generator

For testing DC-motors as generators, two different gear motors are used. The motors are chosen based on certain parameters. The first is the size of the motor. The motor has to be able to fit when the axis of the shaft is aligned with the hinge of an office door as shown in Figure 36. Secondly, the motor may not require too much torque to be rotated. The generator should not cause someone to perceive the door as harder to open. Finally, the motor should not be too expensive as this would defeat part of the purpose of an EH system. The motors that are chosen based on these criteria were the Sparkfun ROB-12285 with a gear ratio of 298:1 and the Igarashi TYP 20G-150 with a gear ratio of 150:1.

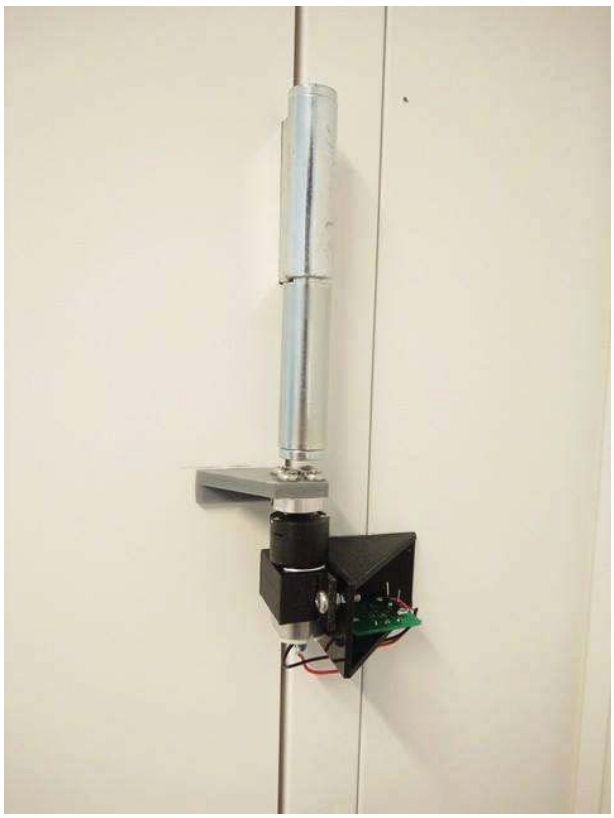

Figure 36. Test set-up of TYP 20G-150 motor with a LTC3588-1 power management board.

To determine the speed of a door opening, a door being opened and closed is filmed. The time stamp of the door being opened and the time stamp of the door being closed is then used. Based on 20 filmed door openings, the mean value of the average revolving speed during a door opening was found to be 9.2 turns per minute. The mean value was used for choosing DC-motors.

Based on the data from *Table 11* in combination with the equations found in chapter 6 the TYP 20G-150 would produce a power of 0.163 W at a rotation speed of 9.2 turns per minute. The ROB-12285 would give 0.046 W based on the data from *Table 11* and with a rotation speed of 9.2 turns per minute.

Table 11. Data for the motors used in the experiment [57] [58].

Motor	R	V_t	I_{nl}	n_{nl}	I_{stall}	P_{out}
ROB-12285	298	12 V	0,07 A	90 rpm	1,6 A	0.046 W
TYP 20G-150	150	12 V	0,06 A	67 rpm	3 A	0.163 W

12.5 Power Management Boards

Two different power management boards are used to test the motors. The LTC3105 circuit used in the PVC tests with the battery protection disconnected and a circuit with LTC3588-1 as shown in Figure 37.

To be able to use the motors with the LTC3105, a rectifier bridge is used. The bridge is made of four rectifier diodes of the type 1N4148 connected as shown in Figure 21 in the Power Control chapter. The Vmppc is set to 0.47 V through connecting a 47 kOhm resistor between the MPPC pin of the LTC3105 and ground. The output voltage is set to 3.2 V.

12.5.1 LTC3588-1

The LTC3588-1 is a combined rectifier and buck-converter with a usable voltage input of 2.7 V to 20 V. The converter is designed for usage with high impedance transducers. There are four different programmable output voltages available of 1.8 V, 2.5 V, 3.3 V and 3.6 V [59]. For the test the 3.6 V output level is chosen. All components used in the electronic design, as seen in Figure 37, are chosen based on recommendations from the LTC3588-1 datasheet. The PCB schematic shown in Figure 37 and Figure 38 is designed in Autodesk Eagle and the prototype ordered from a PCB manufacturer.

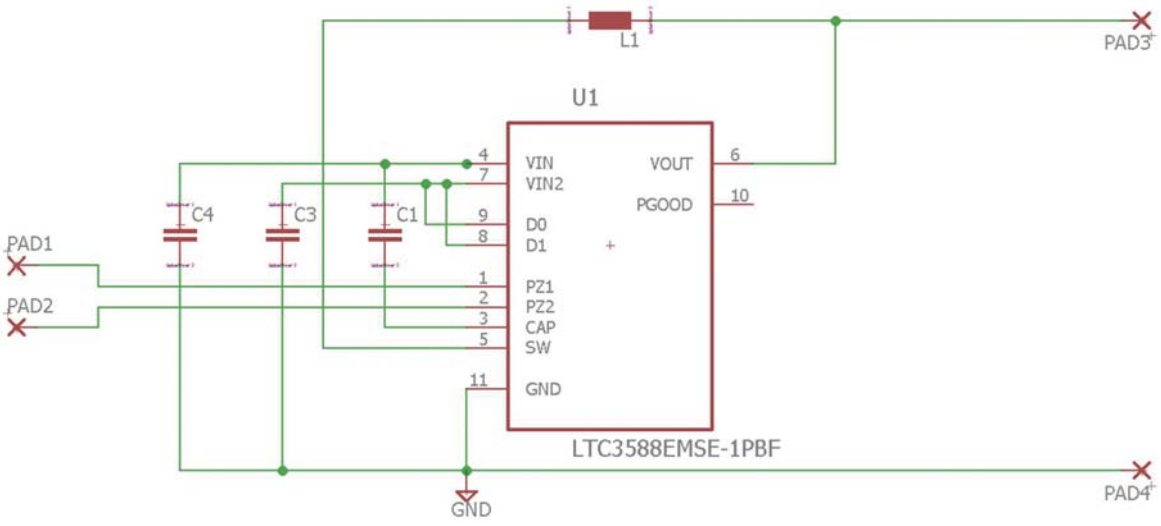

Figure 37. Electronic design of the LTC3588-1 testing board.

L1 is an inductor with 10 μH inductance, C1 is a capacitor with a value of 1 μF, C3 is a 4.7 μF capacitor and C4 has a value of 10 μF.

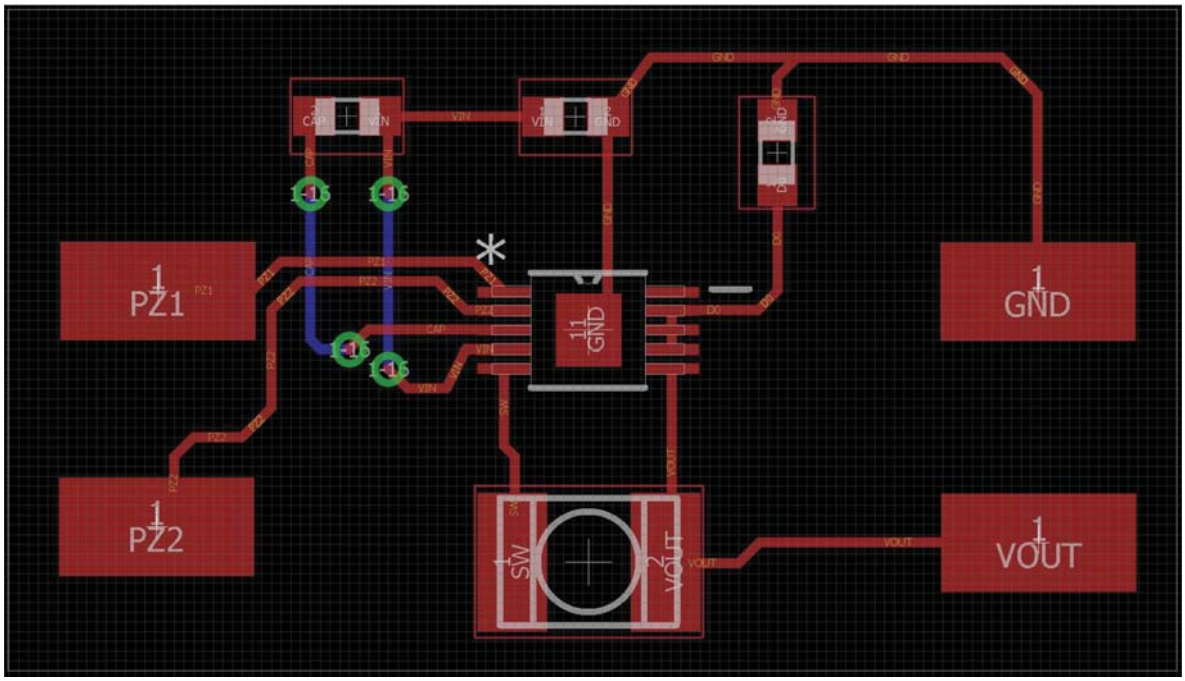

Figure 38. PCB schematic of the LTC3588-1 testing board.

The PZ1 and PZ2 pads in Figure 38 are for voltage input from an AC source. The LTC3588-1 has a built-in rectifier diode bridge. A DC source could be connected directly between the Vin-pin and ground. The VOUT pad is used for adding energy storage and a load to the system. To be able to measure the output energy from the converter, a capacitor of 100 μF is added between VOUT and ground. The amount of energy inserted into the capacitor can be derived from

$$E = \frac{1}{2} C \cdot \left(U_{max}^2 - U_{min}^2\right).$$

12.6 Test Set-up

The tests are carried out on a 205x82.5x4cm wooden office door where the generators are set up beneath the upper hinge of the door as shown in Figure 36 and Figure 39. The torques required to spin the generators are low enough, compared to the torque required to open the door, not to be noticed by people in the office. The velocities the generators are tested at varies between 7.5 rpm and 13.6 rpm depending on the speed people coming in and out of the office opens the door at. The generators are fixed to the door through putting double-sided tape on a 3D-printed fixture clamped around the generators.

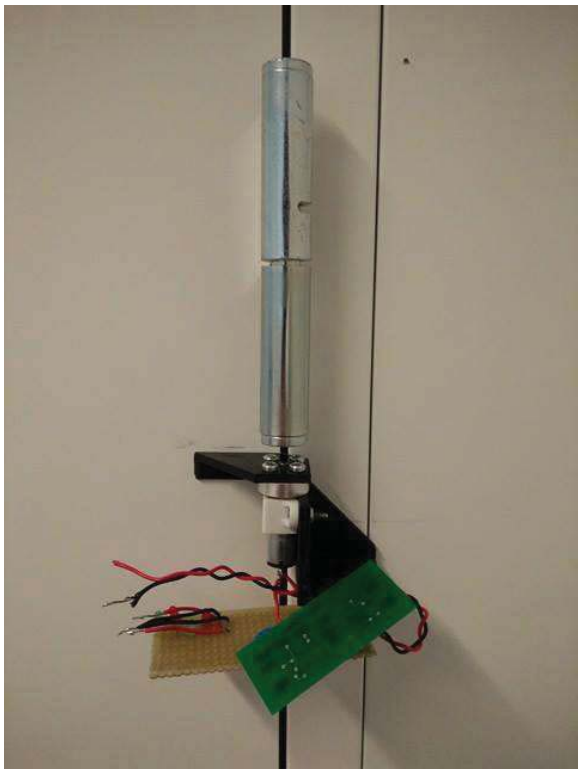

Figure 39. Test set-up of ROB-12285 motor with a rectifier bridge and a LTC3105 power management board.

The power output from the system is obtained through measuring the voltage over a 100 μF capacitor with a voltage rating of 4 V. The LTC3588-1 is programmed to output 3.6 V and the LTC3105 is programmed to output 3.2 V. The LTC3105 has a $Vmppt$ of 470 mV for both motors.

There are also tests carried out with the LTC3105 in combination with the ROB-12285 and a 0.1 F supercapacitor connected as load. In these tests the generator is not mounted on the door but turned by hand to allow for longer motions.

13 Results

13.1 Lux Measurements

The office rooms at Axis without windows have an illuminance of approximately 302 to 372 Lux, but the indoor tests are done at 302 – 346 Lux. The illuminance in the office rooms with windows varies greatly depending on the outdoor light. Measurements shows a variation from about 694 lux on a very foggy day, to 3900 lux on a cloudy day and 54600 lux on a bright sunny day. All measurements are done at about mid-day.

13.2 PVC Tests

LTC3105 has trouble boosting the voltage in low lux environments. Different configurations of PVCs and MPPC resistors are tested but DC conversion does not work unless it is located in a high lux environment like outdoor sunlight. Consequently, only the results from testing with BQ25570 EVM are presented. A distinction between the output power before and after the 1.8 V limit, where the boost converter starts to work efficiently, is made.

The results from testing KXOB22-12X1L in indoor fluorescent office light at 302 – 346 lux, are shown in Table 12.

Table 12. Results from testing KXOB22-12X1L in indoor fluorescent office light at 302-346 lux.

Row	Col	Power before 1.8 V (µW)	Power after 1.8 V (µW)	Total area of PVCs (cm^2)	Power Density after 1.8 V ($\mu W/cm^2$)	Comments
4	3	<10	63.1	18.48	3.42	Trouble getting over 1.8 V, where the boost converter starts to work efficiently
3	4	<10	56.0	18.48	3.03	-
2	6	<10	56.3	18.48	3.05	-

The results from testing AM-1417 in indoor fluorescent office light at 302 – 346 lux, are shown in Table 13.

Table 13. Results from testing AM-1417 in indoor fluorescent office light at 302-346 lux.

Row	Col	Power before 1.8 V (µW)	Power after 1.8 V (µW)	Total area of PVCs (cm^2)	Power Density after 1.8 V ($\mu W/cm^2$)	Comments
2	2	1.10	104	19.46	5.35	
4	1	3.51	152	19.46	7.81	Highest power density

The configuration 1x4 AM-1417 is not tested since the output voltage from the PVCs would be higher than the rated input voltage of BQ25570 EVM.

The 4x1 AM-1417 configuration has the highest power output and power density. The typical charging process of this configuration is shown in Figure 40 and Figure 41. Figure 40 shows the entire charging process and Figure 41 zooms in on the process after 1.8 V.

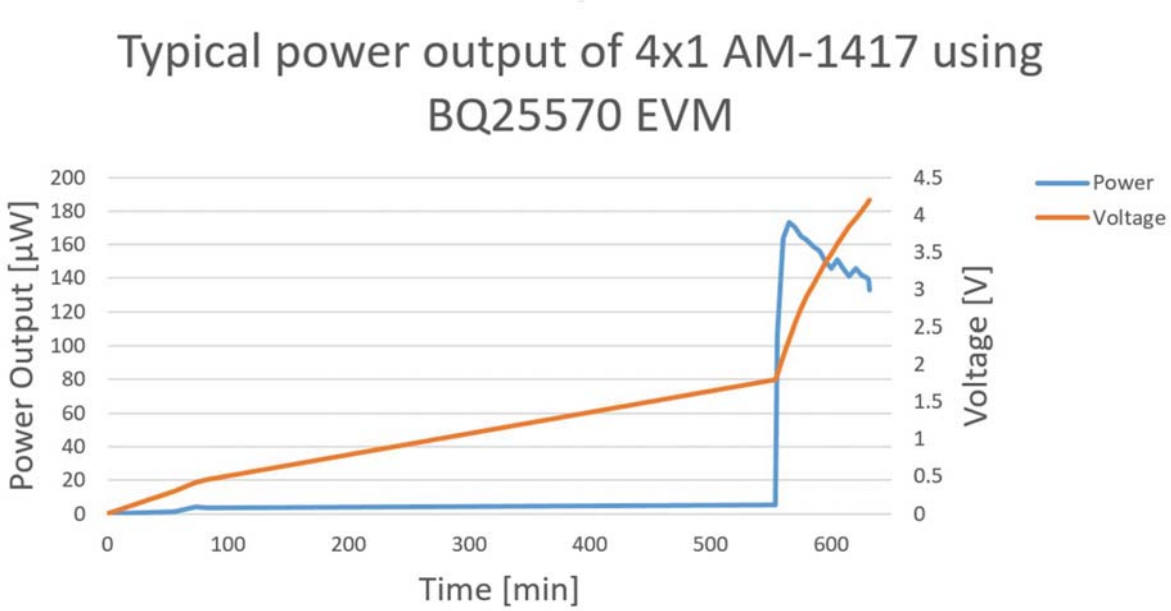

Figure 40. Power output and voltage during a typical charging process of a supercapacitor using 4x1 AM-1417 and BQ25570 EVM at 302-346 lux.

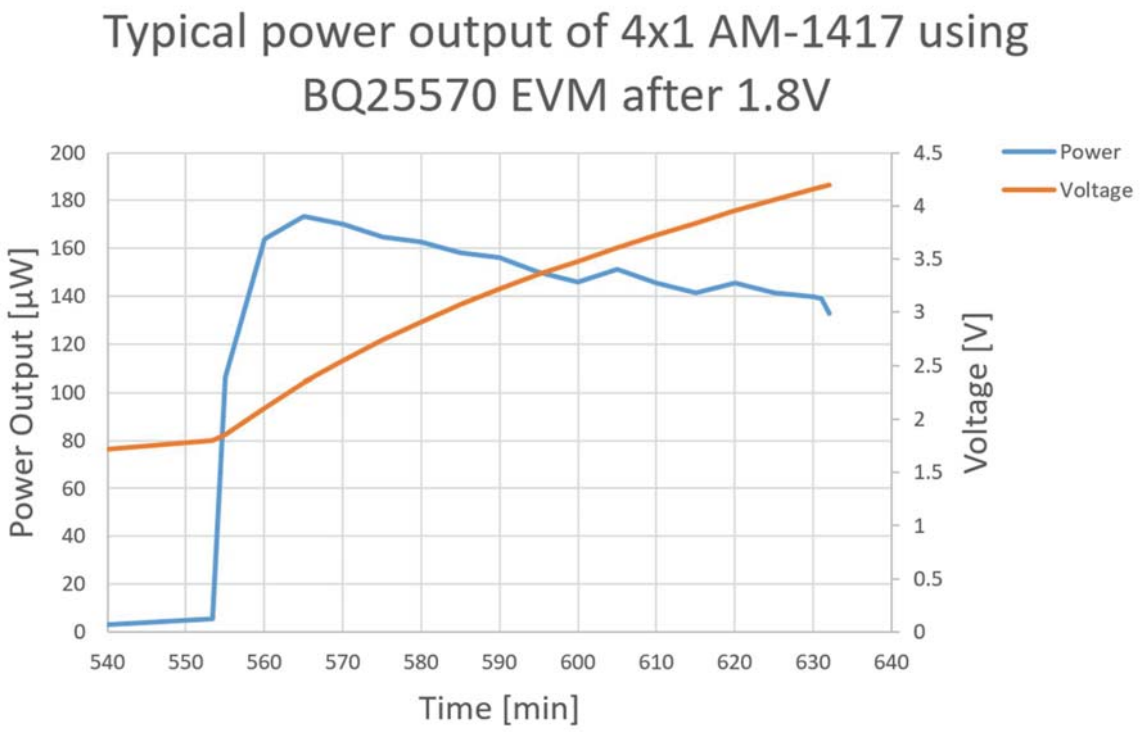

Figure 41. Power output and voltage during a typical charging process of a supercapacitor using 4x1 AM-1417 and BQ25570 EVM after 1.8 V at 302-346 lux.

The results from testing KXOB22-12X1L in bright outdoor light at about 47800 lux are shown in Table 14.

Table 14. Results from testing KXOB22-12X1L in bright outdoor light at about 47800 lux.

Row	**Col**	**Power before 1.8 V (µW)**	**Power after 1.8 V (µW)**	**Total area of PVCs (cm^2)**	**Power Density after 1.8 V ($µW/cm^2$)**	**Comments**
4	3	-	66500	18.48	3600	Difficult to measure before 1.8V accurately because of the low time interval.

The results from testing AM-1417 in bright outdoor light at about at 41 000 to 47800 lux are shown in Table 15.

Table 15. Results from testing AM-1417 in bright outdoor light at 41000 – 47800 lux.

Row	Col	Power before 1.8 V (µW)	Power after 1.8 V (µW)	Total area of PVCs (cm^2)	Power Density after 1.8 V ($\mu W/cm^2$)	Comments
4	1	216	1050	19.46	53.9	

13.3 DC-generator Results

13.3.1 LTC3588-1

When using the generators with the LTC3588-1 the voltage is too low to be usable by the converter, no matter which motor used, and no energy output is registered at the tested speeds.

13.3.2 LTC3105

Using the ROB-122585 with the LTC3105 at an average speed of 11.1 rpm during a door opening results in the voltage over the capacitor shown in Figure 42. The voltage over the capacitor rises from 1.04 V to 3.12 V resulting in at least an energy output of 433 µJ. At speeds below this the energy output will be zero.

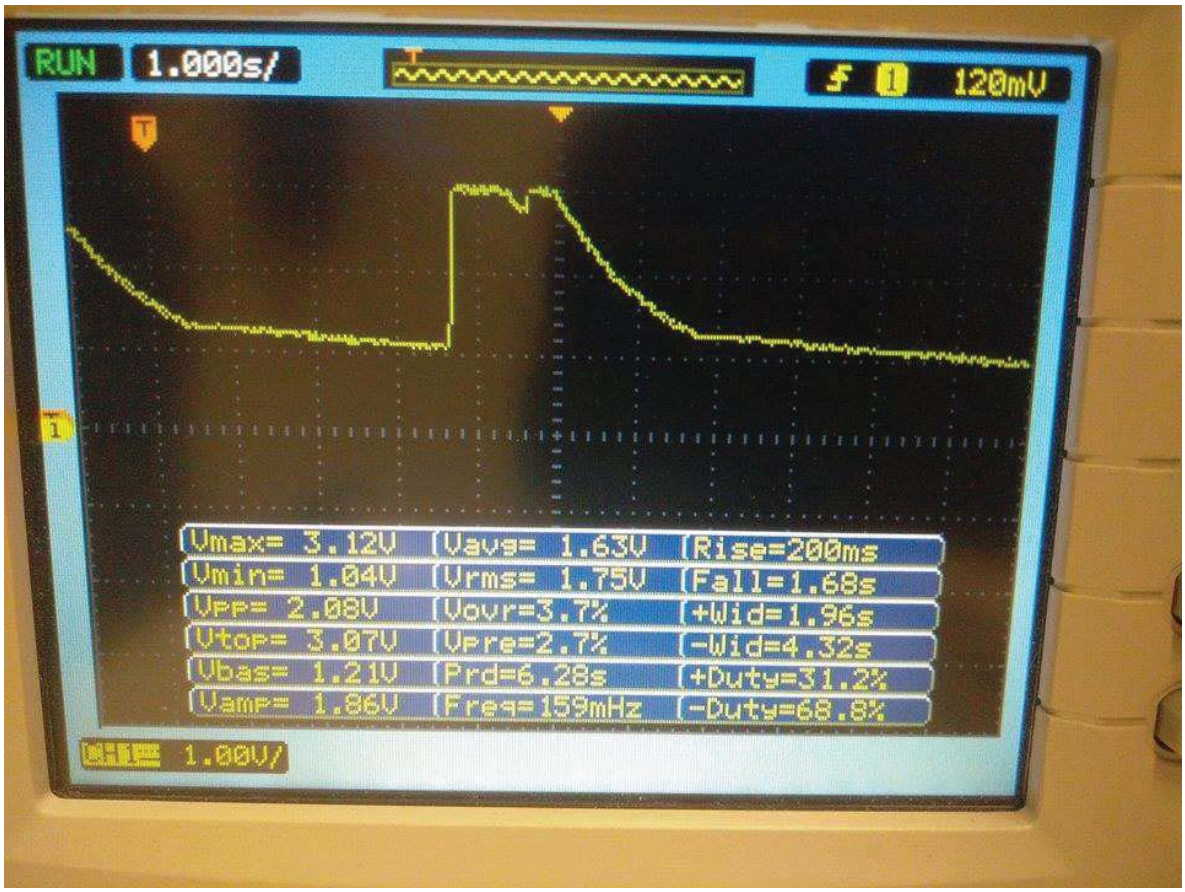

Figure 42. Voltage over time measured at the GND and the VOUT pads of the LTC3105 board with a ROB-12285 connected to a rectifier board used to supply power. The voltage is measured over a 100 µF capacitor.

Using the TYP 20G-150 instead results in the graph shown in Figure 43. The generator is spun at approximately the same average speed. The voltage over the capacitor increases from 0.64 V to 3.12 V

resulting in, at least, an energy output of 467 µJ. Energy can be extracted from the generator at speeds as low as 7.5 rpm as seen in Figure 44.

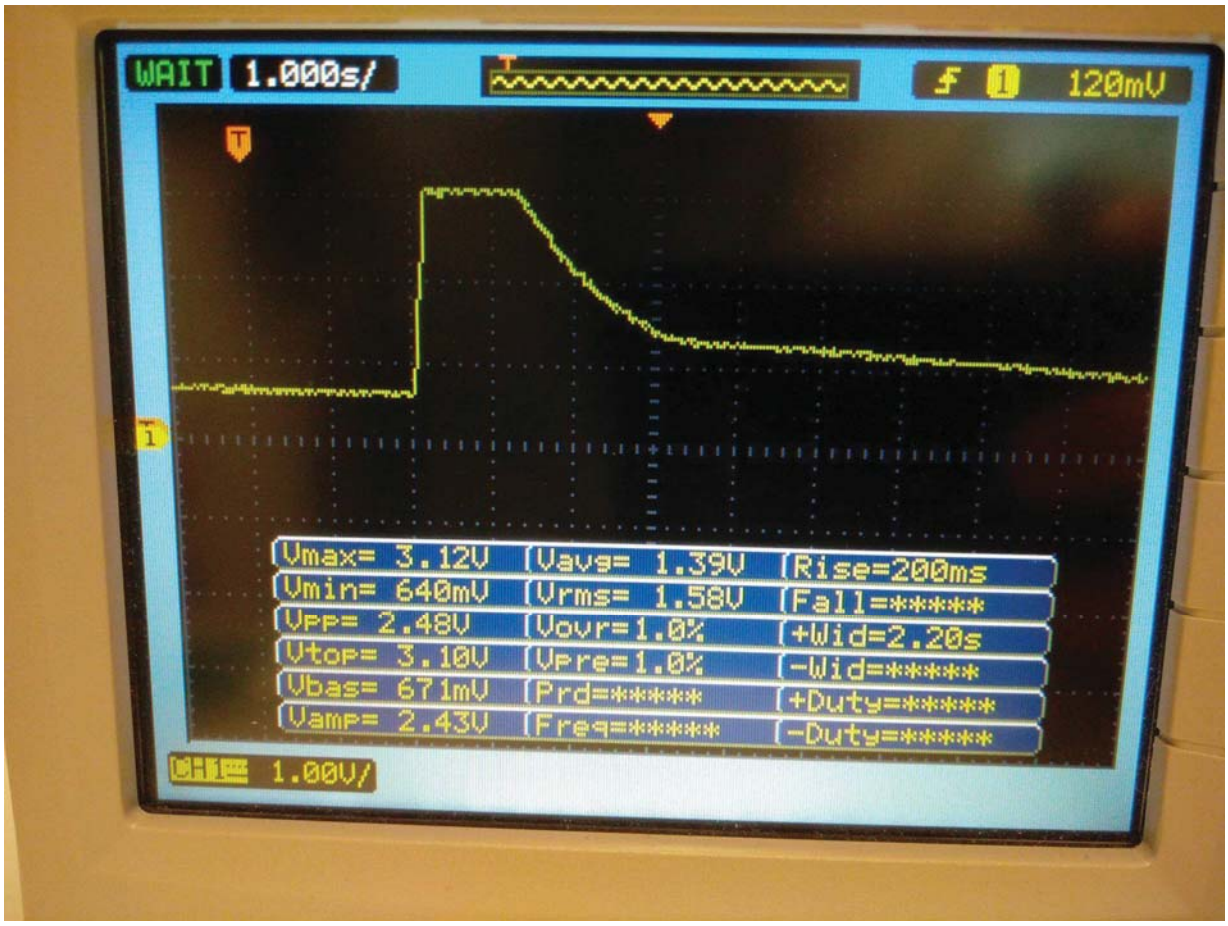

Figure 43. Voltage over time measured at the GND and the VOUT pads of the LTC3105 board with a TYP 20G-150 motor connected to a rectifier board used to supply power. The voltage is measured over a 100 µF capacitor.

Figure 44. Voltage over time measured at the GND and the VOUT pads of the LTC3105 board with a TYP 20G-150 motor connected to a rectifier board used to supply power. The voltage is measured over a 100 µF capacitor.

When using a supercapacitor of 0.1 F, the voltage levels seen in Figure 45 are achieved. In this case the generator turns 180 degrees instead of the normal 90 degrees of a door opening motion. The average speed of the motion is 18.75 rpm with a starting voltage of about 5 mV and an end voltage of about 14mV resulting in a total energy gain of 171 µJ.

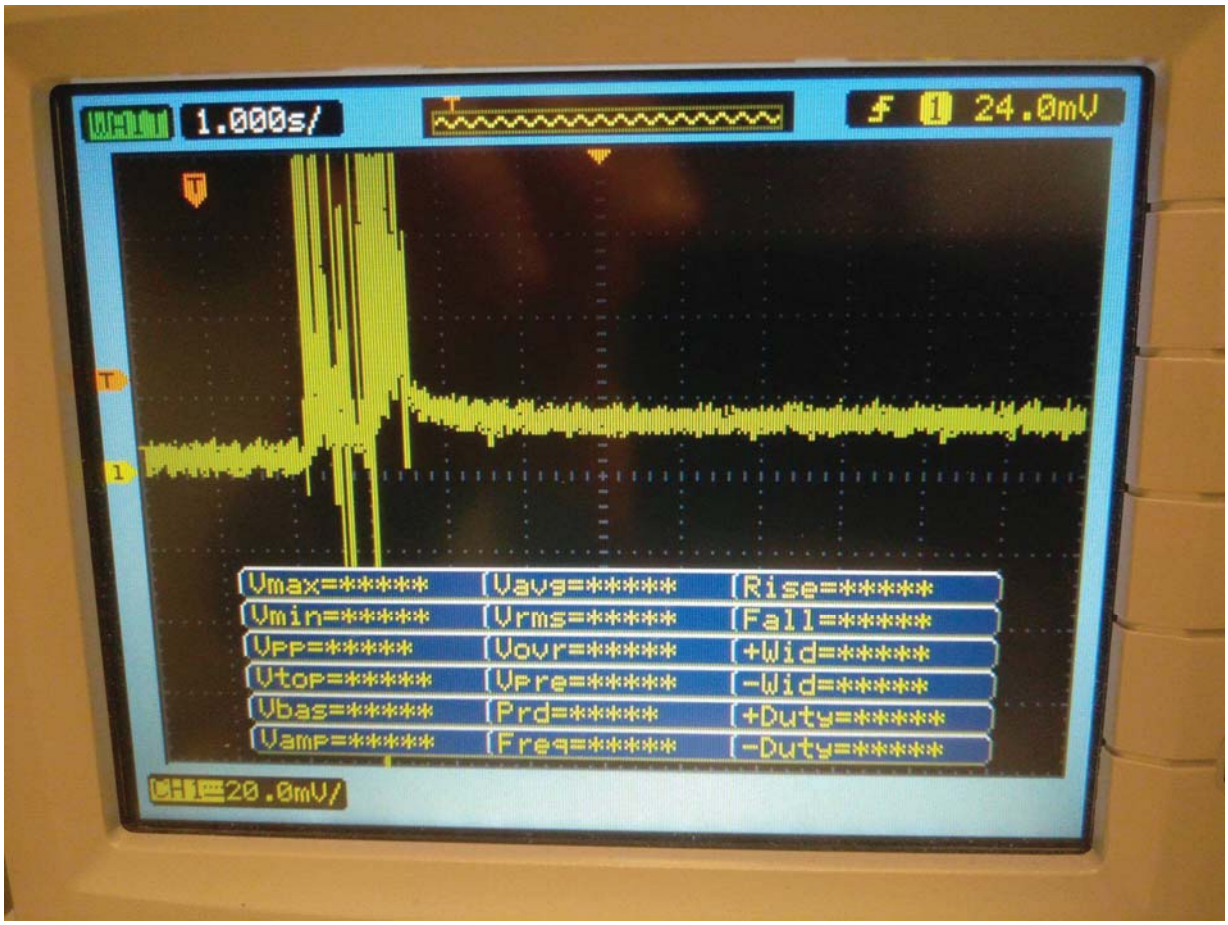

Figure 45. Voltage over time measured at the GND and the VOUT pads of the LTC3105 board with a ROB-12285 connected to a rectifier board used to supply power. The voltage is measured over a 0.1 F supercapacitor.

14 Discussion

It is noted in the theory chapters that some EH technologies are more practical than others. Vibration based methods requires very specific conditions to function. They may be applied in environments where the vibrations are known and fairly constant, for example in laboratory environments or close to large machines. Another indicator of the relatively low usability is the low amount of commercially available vibration transducers. TEGs requires specific thermal conditions which are not found in most environments. However, they can be useful if the right thermal conditions are available. This is seen in the automotive industry's interest in implementing TEGs in combustion engines. The practical limitations of the TEGs are the reason they are not further investigated in this thesis. RF EH is a popular area with expectations not yet aligned with reality. The efficiency of an RF transducer is high, but it is hard to apply to an application considering the low amount of energy that is available. PVCs are relatively easy to use and it is not difficult to find an environment with a sufficient amount of energy for a practical purpose.

Electromagnetism has proven to be a useful method for harvesting mechanical energy. EnOcean's ECO 200 is a functioning commercial example of this. It is applicable in almost any environment since it only requires the push of a button.

In the indoor PVC test results, Table 12 and Table 13, it is seen that AM-1417 works better than KXOB22-12X1L in indoor fluorescent office light. This is to be expected since AM-1417 is an amorphous PVC. The best configuration is 4x1. This is reasonable since one AM-1417 gives a 1.5 V operating voltage at 200 lux, which is more than enough for BQ25570 330 mV cold start-up limit. The parallel coupling of the PVCs increases the operating current, which is low at $12.5*10^{-5}$ A per AM-1417 at 200 lux. The outdoor test results, Table 14 and Table 15, shows that KXOB22-12X1L works significantly better than AM-1417 in outdoor sunlight, which is to be expected since it is a monocrystalline PVC. However, the power density of 3600 $\mu W/cm^2$ cannot be expected every day since it requires bright sunlight, but the results confirms the behavior of monocrystalline and amorphous PVCs. The results also demonstrate what a difference sunlight can make.

Figure 40 and Figure 41 shows that the EH system consisting of 4x1 AM-1417, BQ25570 EVM and the supercapacitor should be used above the 1.8 V interval, where the boost charger starts to work efficiently. This gives an average power of 152 µW, or 130 µW at its lowest, which is enough to power most low power MCUs which spend most of their time in a low energy mode. As long as the lights are on and the PVCs are not placed in shadow, 130 µW can be seen as a bad-case-scenario. Any sunlight hitting the PVCs from windows will result in a higher power output. The test results should not be considered as exact since it was difficult to find an environment with a constant illuminance.

LTC3105's inability to boost the voltage when testing the PVCs may be because of factors like the burst mode operation or the constant voltage method used by the MPPC draws too much power. Since EH applications are supposed to work in indoor environments, the tests with LTC3105 are discarded.

The tests done with the DC-generators together with the LTC3588-1 are inconclusive as the voltage levels achieved are not high enough to use with the IC. The 2.7 V minimum input level is not achievable with the DC-generators at normal door opening speeds. Since there is no programmable MPPT for the IC and DC motors have a low impedance the energy transfer from the generator is probably very low. The

maximum open circuit voltage of the motors during the tests lies around 4 V. This means that at the maximum power point the IC has a 2 V potential difference. However, since the impedance of the IC is higher than the DC generator and unable to change, the potential over the IC is in theory higher than those 2 V. The mismatch in impedance probably causes the efficiency of the system to be very low.

Using a DC-generator with the LTC3105 provides usable energy levels though they are far from the theoretical values. Both motors are able to charge a 100 µF capacitor in a fraction of a door opening at reasonable speeds. The total energy required to charge the capacitor from the measured values were 433 and 467 µJ. Compared to the 120 µJ the push-button device from EnOcean required to send a signal, these are usable energy levels as long as the power during the load interval is sufficient. Looking at Figure 42 and Figure 43 it is obvious there is more energy to extract from the door opening process. Unfortunately there was no access to a capacitor of suitable size during the tests.

A problem when adding a load to the EH application is to be able to connect and disconnect the load at set times. In this case the energy extracted is probably sufficient to power the kind of transceiver used in the push-button device long enough to send a signal. However, since the energy levels of the system are so small, using some sort of switch to be able to disconnect the load during the EH-process would be preferable. In the case of a door opening this could be achieved through connecting a contact switch between the door and the wall. This would allow the system to power the load after a full 90 degree door opening giving the application a lot more reliability. Still, since the door opening motion could be done at varying velocities, and the energy output is so susceptible to velocity, there is no guarantee an EH application would be able to perform a given task from a single door opening. The minimum speed for acquiring a usable voltage level could be lowered somewhat by using a more efficient rectifier bridge. For example through replacing the 1N4148 diodes with schottky diodes or a MOSFET based rectifier with lower forward voltage.

In theory the MPP for an ideal DC generator with an open circuit voltage of 4 V would be at 2 V. However, in the tests a diode bridge rectifier with 1 V forward voltage per diode are added. Since the LTC3105 is using a sort of constant voltage MPPT a voltage level slightly above the minimum level required to drive the converter is used. Using a higher voltage level for the MPPT would result in a worse efficiency due to worse power transfer. A forward voltage beneath 0.875 V would have made it possible, in theory, to reach the MPP.

The reliability, or the possibility of an EH system not receiving sufficient energy to complete tasks is one of the greater challenges of EH. Since, in practice, all of the energy sources for the EH transducers are fluctuating or unreliable there is a need to have either a high marginal or strictly controlled energy levels being transduced to the applications. Having controlled energy levels requires the EH systems to be tailored to their load. Here, changing the load most likely means exchanging the entire EH system.

The tests done with supercapacitors showed lower energy output results than having a ceramic capacitor. The problem might arise from the high current required to charge the capacitor at low voltage or possibly from some oscillation in the system due to the large ESR of the supercapacitor. This could also be elevated as a result of the “burst mode” operation of the LTC3105 as this causes the power output to the supercapacitor to spike during short intervals.

Another problem during the tests was the stress acting on the gears in the gearbox. A part of the tension came from the alignment of the generators with the hinges. If the generator is poorly aligned, the gearbox breaks after a few cycles.

15 Conclusions and Future Work

This thesis focuses on the potential energy available for EH applications. This is only half the problem, since the load power requirement also is of significance. An interesting area for future research would therefore be on the power requirements of loads suitable for EH applications.

EH transducers provides varying voltage and current outputs and this puts specific demands on the ICs. DC-DC converters and battery protections can be developed further to be more adapted to EH applications. A market investigation over the EH voltage converter ICs available today could be done to provide insight into which ICs provide the best efficiency for which application.

An economical investigation about the potential cost savings when using EH could be useful for motivating an increased use.

A life cycle analysis could be done for small scale PVC systems to investigate if using PVCs in combination with a battery leaves a smaller ecological footprint than just using a battery to power an EH application.

The efficiency of using the PVCs together with a load and a li-ion battery should be investigated since it might differ with a battery storage. A study over what effect the placement and the lighting type has on the energy output of the PVC could also be done.

Since the gearbox of the DC-generators were prone to break due to misalignment, a more flexible way of mounting the prototype could be developed. Also, a much more efficient EH system better matched for the generators could be made. Finally, a suitable load and energy storage for the application could be established where the load is matched to the prototype.

16 References

[1] H. Venkataraman and G.-M. Muntean, Green Mobile Devices and Networks, Boca Raton, Florida: CRC Press, 2012.

[2] P. Spies, L. Mateu and M. Pollak, Handbook of Energy Harvesting Power Suppiles and Applications, Boca Raton, Florida: CRC Press, 2013.

[3] Enerpoint, "The photovoltaic cell," [Online]. Available: http://www.enerpoint.co.uk/photovoltaic_technology.php. [Accessed 3 28 2017].

[4] Solarbotics, "Solar Cells," 2002. [Online]. Available: http://solarbotics.net/starting/200202_solar_cells/200202_solar_cell_physics.html. [Accessed 28 3 2017].

[5] J. Nelsson, The Physics of Solar Cells, London: Imperial College Press, 2003.

[6] Panasonic, "Amorton," [Online]. Available: https://panasonic.co.jp/es/pesam/en/products/pdf/Catalog_Amorton_ENG.pdf. [Accessed 3 May 2017].

[7] Texas Instruments, "BQ25570," [Online]. Available: http://www.ti.com/lit/ds/slusbh2e/slusbh2e.pdf. [Accessed 20 April 2017].

[8] D. Freeman, "Introduction to Photovoltaic Systems Maximum Power Point Tracking," November 2010. [Online]. Available: http://www.ti.com/lit/an/slva446/slva446.pdf. [Accessed 24 April 2016].

[9] Energy Informative, "Energy Informative - best solar panel monocrystalline polycrystalline thin film," [Online]. Available: http://energyinformative.org/best-solar-panel-monocrystalline-polycrystalline-thin-film/. [Accessed 28 3 2017].

[10] Energy Informative, "Energy Informative - solar cell comparison chart mono polycrystalline thin film," [Online]. Available: http://energyinformative.org/solar-cell-comparison-chart-mono-polycrystalline-thin-film/. [Accessed 28 3 2017].

[11] IXYS, "IXYS KXOB22-12X1L," 20 April 2017. [Online]. Available: http://ixapps.ixys.com/DataSheet/KXOB22-12X1L-DATA-SHEET-20130902-.pdf.

[12] M. A. Green, E. Keith, Y. Hishikawa, W. Warta, E. D. Dunlop, D. H. Levi and A. W. Y. Ho-Baille, "Solar cell efficiency tables (version 49)," *Progress in Photovoltaics: Research and Applications,* vol. 25, no. 1, pp. 3-13, 2017.

[13] Arbetsmiljöverket, "Arbetsmiljöverket," 2016. [Online]. Available: https://www.av.se/inomhusmiljo/ljus-och-belysning/belysning-pa-kontor/. [Accessed 4 3 2017].

[14] C. Bach, "New Indoor light source trends and their impact on classical photovoltaic harvester (indoor a-Si solar cells) yield," 2015. [Online]. Available: https://www.enocean.com/en/technology/white-papers/. [Accessed 24 April 2017].

[15] R. Calio, U. B. Rongala, D. Camboni, M. Milazzo, C. Stefanini, G. de Petris and C. M. Oddo, Piezoelectric Energy Harvesting Solutions, Basel: MPDI, 2014.

[16] W. J. Wu and B. S. Lee, Piezoelectric MEMS Power Generators for Vibration Energy Harvesting, Taipei: InTech, 2012.

[17] S. J. Roundy, Energy Scavenging for Wireless Sensor Nodes with a Focus on Vibration of Electricity Conversion, Berkeley: University of California, 2003.

[18] K. Sang-Gook, S. Priya and I. Kanno, Piezoelectric MEMS for Energy Harvesting, Cambridge University Press (Materials Research Society), 2012.

[19] N. S. Schenck and J. A. Paradiso, Energy Scavenging with Shoe-Mounted Piezoeletrics, IEEE, 2001.

[20] C. Y. Schu and I. C. Lien, Efficiency of Energy Conversion for a Piezoelectric Power Harvesting System, IOP Publishing Ltd, 2006.

[21] C. T. Pan, Y. M. Hwang, L. Liwei and C. Ying-Chung, Design and Fabrication of Self-Powered Micro-Harvesters, Singapore: John Wiley & Sons, 2014.

[22] M. El-hami, P. Glynne-Jones, N. White, M. Hill, S. Beeby, E. James, A. Brown and J. Ross, "Design and fabrication of a new vibration-based electromechanical power generator," *Sensors and Actuators A: Physical,* vol. 92, no. 1-3, pp. 335-342, 2001.

[23] EnOcean, "Energy Harvester ECO 200," August 2015. [Online]. Available: https://www.enocean.com/en/enocean_modules/eco-200/. [Accessed 24 April 2017].

[24] F. Schmidt, "Energy harvesting at the press of a button," 26 November 2012. [Online]. Available: http://www.eetimes.com/document.asp?doc_id=1280156&page_number=1. [Accessed 24 April 2017].

[25] D. H. Litwhiler and T. H. Gavigan, A Door Motion Energy Harvesting System for Powering an Electronic Door Lock, Penn State, Berks, 2014.

[26] K. Mimis, D. Gibbins, S. Dumanli and G. T. Watkins, "Ambient RF Energy Harvesting Trial in Domestic Settings," *IET Microwaves, Antennas & Propagation,* vol. 9, no. 5, pp. 454-462, 2015.

[27] G. D. Durgin and C. R. Valenta, "Harvesting Wireless Power: Survey of Energy-Harvester Conversion Efficiency in Far-Field, Wireless Power Transfer Systems," *IEEE Microwave Magazine,* vol. 15, no. 4, pp. 108-120, 2014.

[28] Micropelt, "Micropelt," [Online]. Available: http://micropelt.com/. [Accessed 25 April 2017].

[29] TEGnology, "TEGnology," [Online]. Available: http://tegnology.dk/p/concept. [Accessed 5 May 2017].

[30] J. Wardlaw and A. Karsilayan, "Self-Powered Rectifier for Energy Harvesting Applications," *IEEE Journal on Emerging and Selected Topics in Circuits and Systems,* vol. 1, no. 3, pp. 308-320, 2011.

[31] E. A. Gomez-Casseres, S. M. Arbulú, R. J. Franco, R. Contreras and J. Martínez, "Comparison of Passive Rectifier Circuits for Energy Harvesting Applications," in *IEEE Canadian Conference on Electrical and Computer Engineering*, Vancouver, BC, 2016.

[32] Y. Kushino and K. Hirotaka, "Piezoelectric Energy Harvesting Circuit Using Full-Wave Voltage Doubler Rectifier and Switched Inductor," in *Energy Conversion Congress and Exposition*, Pittsburgh, PA, 2014.

[33] T. Kashiwao, I. Iman, L. Yee Yan and M. Deguchi, "Optimization of rectifier circuits for a vibration energy harvesting system using a macro-fiber composite piezoelectric element," *Microelectronics Journal,* vol. 54, pp. 109-115, 2016.

[34] J. Segura and C. F. Hawkins, CMOS Electronics: How It Works, How It Fails, Wiley-IEEE Press, 2004.

[35] H. Goncalves, M. Martins and J. Fernandes, "A study on MOSFET rectifiers with transistors operating in the weak inversion region," in *2012 19th IEEE International Conference on Electronics, Circuits and Systems*, Seville, Spain, 2012.

[36] S. S. Hashemi, M. Sawan and S. Yvon, "A High-Efficiency Low-Voltage CMOS Rectifier for Harvesting Energy in Implantable Devices," *IEEE Transactions on Biomedical Circuits and Systems,* vol. 6, no. 4, pp. 326-335, 2012.

[37] C. Peters, F. Henrici, M. Ortmanns and Y. Manoli, "High-Bandwidth Floating Gate CMOS Rectifiers with Reduced Voltage Drop," in *IEEE International Symposium on Circuits and Systems*, Seattle, WA, 2008.

[38] J.-P. Curty, M. Declercq, C. Dehollain and N. Joehl, Design and Optimization of Passive UHF RFID Systems, Springer US, 2007.

[39] K.-H. Chen, Power Management Techniques for Integrated Circuit Design, Wiley-IEEE Press, 2016.

[40] Y. Wu, Lithium-Ion Batteries: Fundamentals and Applications, CRC Press 2015, 2015.

[41] J.-M. Tarascon, Electrochemical Energy Storage, London: Wiley, 2015.

[42] D. Larcher and J.-M. Tarascon, "Towards Greener and More Sustainable Batteries for Electrical Energy Storage," *Nature Chemistry,* vol. 7, no. 1, pp. 19-29, 2015.

[43] M. Braga, N. Grundish, A. Murchison and J. Goodenough, "Alternative Strategy for a Safe Rechargeable Battery," *Energy & Environmental Science,* vol. 10, no. 1, pp. 331-336, 2017.

[44] V. S. Bagotskii, A. M. Skundin and Y. V. Volfkovich, Electrochemical Power Sources : Batteries, Fuel Cells, and Supercapacitors, Hoboken, New Jersey: Wiley, 2014.

[45] F. Béguin and E. Frackowiak, Supercapacitors: Materials, Systems, and Applications, Weinhiem: Wiley-VCH, 2013.

[46] A. Kansal, D. Potter and M. Srivastava, "Performance Aware Tasking for Environmentally Powered Sensor Networks," in *ACM Joint International Conference on Measurments and Modeling of Computer Systems*, 2004.

[47] A. Kansal, J. Hsu, S. Zahedi and M. B. Srivastava, "Power Management in Energy Harvesting Sensor Networks," *ACM Transactions on Embedded Computing Systems,* vol. 6, no. 4, 2007.

[48] Silicon Labs, "Manage the IoT on an Energy Budget," 2017. [Online]. Available: http://www.silabs.com/whitepapers/manage-the-iot-on-an-energy-budget. [Accessed 4 April 2017].

[49] A. Guldahl, "Understanding MCU sleep modes and energy savings (white paper)," 6 March 2016. [Online]. Available: http://www.embedded.com/design/power-optimization/4237635/Understanding-MCU-sleep-modes-and-energy-savings. [Accessed 4 April 2017].

[50] Freescale Semiconductor, "Freescale Energy - Efficient Solutions: Kinetis L Series MCUs," 12 November 2014. [Online]. Available: http://cache.nxp.com/assets/documents/data/en/white-papers/ENEFFSOLKINLSWP.pdf?fsrch=1&sr=2&pageNum=1. [Accessed 4 April 2017].

[51] Silicon Labs, "Top 10 Silicon Labs 32-bit Microcontroller Technology Features," 2017. [Online]. Available: http://www.silabs.com/products/mcu/32-bit/32-bit-microcontroller-technology. [Accessed 4 April 2017].

[52] Panasonic, "Amorton Product Info," [Online]. Available: https://panasonic.co.jp/es/pesam/en/products/. [Accessed 20 April 2017].

[53] Linear Technology, "LTC3105," [Online]. Available: http://cds.linear.com/docs/en/datasheet/3105fb.pdf. [Accessed 20 April 2017].

[54] Linear Technology, "LTC4071," [Online]. Available: http://cds.linear.com/docs/en/datasheet/4071fc.pdf. [Accessed 20 April 2017].

[55] Texas Instruments, "BQ25570 EVM," [Online]. Available: http://www.ti.com/lit/ug/sluuaa7a/sluuaa7a.pdf. [Accessed 20 April 2017].

[56] SEKONIC, "Flash Master L-358," [Online]. Available: http://www.sekonic.com/downloads/l-358_english.pdf. [Accessed 20 April 2017].

[57] Igarashi Motoren GMBH, "Conrad," [Online]. Available: http://www.produktinfo.conrad.com/datenblaetter/225000-249999/244171-da-01-ml-Getriebemotor_1_150_20G_de_en.pdf. [Accessed 27 04 2017].

[58] Sparkfun, "Sparkfun," [Online]. Available: https://www.sparkfun.com/products/12285. [Accessed 27 April 2017].

[59] Linear Technology, "LTC 3588-1," 2010. [Online]. Available: http://cds.linear.com/docs/en/datasheet/35881fc.pdf. [Accessed 26 04 2017].

[60] D. C. Jordan, S. R. Kurtz, K. VanSant and J. Newmiller, "Compendium of photovoltaic degredation rates," *Progress in Photovoltaics: Research and Applications,* vol. 24, no. 7, pp. 978-989, 2016.

[61] Texas Instruments, "MSP430FR599x, MSP430FR596x Mixed-Signal Microcontrollers," [Online]. Available: http://www.ti.com/lit/ds/symlink/msp430fr5962.pdf. [Accessed 21 April 2017].

[62] Silicon Labs, "EFM8 Sleepy Bee Family - EFM8SB1 Data Sheet," [Online]. Available: http://www.silabs.com/documents/public/data-sheets/efm8sb1-datasheet.pdf. [Accessed 21 April 2017].

[63] Texas Instruments, "MSP430xx11x2, MSP430x12x2 Mixed Signal Microcontroller," [Online]. Available: http://www.ti.com/lit/ds/symlink/msp430f1232.pdf. [Accessed 21 April 2017].

[64] Silicon Labs, "EFM32G200 Datasheet," [Online]. Available: http://www.silabs.com/documents/public/data-sheets/EFM32G200.pdf. [Accessed 21 April 2017].

[65] Energy Informative, "Energy Informative - Amorphous silicon solar panels," [Online]. Available: http://energyinformative.org/amorphous-silicon-solar-panels/. [Accessed 29 3 2017].